Giant-atom dephasing dynamics and entanglement generation in a squeezed vacuum reservoir

Xian-Li Yin [1,*] Heung-wing Joseph Lee,[1,†] and Guofeng Zhang [2,3,‡]

[1]*Department of Applied Mathematics, The Hong Kong Polytechnic University, Kowloon 999077, Hong Kong, China*

[2]*Department of Applied Mathematics, The Hong Kong Polytechnic University, Kowloon 999077, Hong Kong, China and The Hong Kong Polytechnic University Shenzhen Research Institute, Shenzhen, Guang Dong 518057, China*

[3]*Research Institute for Quantum Technology, The Hong Kong Polytechnic University, Hong Kong, China*

(Received 3 December 2024; accepted 3 March 2025; published 13 March 2025)

The study of atomic behaviors in a squeezed vacuum reservoir plays an important role in exploring quantum effect and quantum physics. We here propose a scheme to manipulate the dynamics of giant atoms coupled to a one-dimensional waveguide driven by a broadband squeezed field, which acts as a squeezed vacuum reservoir. By tuning the propagating phase of photons, the center-of-mass phase of the giant atom, and the squeezing parameter, both the dephasing dynamics and entanglement dynamics of giant atoms can be effectively controlled. In the single-giant-atom case, we obtain the expressions of the dephasing rates based on the Bloch equations derived from the quantum master equation of the giant atom. Adjusting these two phases enables the dephasing rates to be enhanced, suppressed, or reduced to zero, thereby changing the dephasing dynamics. For the two-giant-atom system, we find that the atomic individual and collective squeezing depend on these two phases simultaneously. The steady-state giant-atom population and entanglement are obtained by working in the collective state representation for the two atoms. Different from small atoms, the steady-state population and entanglement depend on not only the center-mass-of phase, but also the propagating phase. In addition, we identify the condition for achieving larger steady-state entanglement via analyzing the system parameters. This work will facilitate the study of light-matter interaction based on giant-atom waveguide QED systems driven by a squeezed vacuum reservoir and has potential applications in quantum information processing.

DOI: 10.1103/PhysRevA.111.033707

I. INTRODUCTION

Recent advancements in quantum optics have introduced the concept of "giant atoms," which breaks down the traditional dipole approximation from a global viewpoint [1]. This is realized by engineering nonlocal interactions between artificial atoms and microwave [2–4] or acoustic fields [5–7], leading to a new platform for studying the light-matter interactions, called giant-atom waveguide quantum electrodynamics (QED). Unlike conventional waveguide QED [8–11], where atoms interact locally with the electromagnetic fields in the waveguide, giant atoms interact with the fields in the waveguide at multiple points. The distances between these coupling points can be comparable to or much larger than the field wavelengths. This nonlocal coupling leads to a variety of interesting physical phenomena, such as frequency-dependent atomic relaxation rates and Lamb shifts [12,13], non-Markovian dynamics [7,14–22], the formation of decoherence-free subspaces [2,23–27], exotic atom-photon bound states [28–34], and advanced few-photon scattering [35–42]. These effects not found in small atoms open new avenues for fundamental physics and quantum information processing.

Nevertheless, in most existing studies on giant atoms, the field modes in the waveguide are considered to be ordinary vacuum. In these works, the frequency shift, dipole-dipole interaction, individual decay, and collective decay of giant atoms can be controlled by adjusting the coupling-point distances. This results in rich quantum interference effects, which in turn influence the decay dynamics of a single giant atom [7,12–15,17] and the generation of quantum entanglement in two or more giant atoms [43–48]. Meanwhile, single or multiple small atoms in the squeezed vacuum reservoir have also been studied, such as the atomic phase decay [49], prediction and probe of the fluorescence spectrum [50,51], spontaneous emission [52,53], and generating steady state [54–57]. In particular, it has been found that when the fields are driven by a squeezed vacuum reservoir, the center-of-mass coordinate of atoms can affect the collective squeezing related to the two-photon decay process [53–55]. Despite these studies, the dynamics and steady-state behavior of giant atoms coupled to a one-dimensional (1D) waveguide driven by a squeezed vacuum reservoir remain unexplored. The simultaneous manipulation of the squeezing effect and quantum interference effect in giant atoms is still an interesting topic.

In this paper, we combine these two effects to study the decay dynamics and steady-state behavior of giant atoms coupled to a 1D waveguide, where the waveguide is driven by a broadband squeezed vacuum field. Concretely, we consider the cases of a single and two giant atoms, respectively. Using the collisional model method [24,58], the quantum master equation of these two cases is obtained. In the single-giant-atom case, the dephasing rates can be enhanced, suppressed,

*Contact author: xianliyin@foxmail.com
†Contact author: joseph.lee@polyu.edu.hk
‡Contact author: guofeng.zhang@polyu.edu.hk

 ©2025 American Physical Society

or reduced to zero via tuning both the propagating phase and the center-of-mass phase, which correspond to the coupling-point distances and the center-of-mass coordinate of the giant atoms, respectively. It is shown that the dephasing dynamics can exhibit behaviors such as exponential decay and Rabi oscillations or remain unchanged over time. In the two-giant atom case, both the giant-atom individual squeezing and collective squeezing induced by the squeezed vacuum reservoir depend on the propagating phase and center-of-mass phase. We analyze in detail the influence of these two phases on the population and entanglement dynamics, as well as their steady-state behavior. When there is no initial population in the dark state of the two giant atoms, the generated entanglement approaches the same stationary value for different atomic initial states. However, different from small atoms [54], we show that the steady-state atomic entanglement depends on the propagating phase. Meanwhile, we find that the steady-state entanglement is more sensitive to the center-of-mass phase.

The rest of this paper is organized as follows. In Sec. II, we analyze the dephasing dynamics of a single giant atom driven by a squeezed vacuum reservoir in a 1D waveguide. We investigate the influence of the propagating phase, center-of-mass phase, and squeezed parameter on the atomic dephasing rates and dynamics. In Sec. III we extend our analysis to the two-giant-atom case, where we study the atomic population and entanglement dynamics and their steady-state behavior. We also calculate the fidelity between the final state and the target state. Finally, we present a brief discussion and conclusion in Sec. IV. Two Appendixes are provided: the first derives the quantum master equation for giant atoms driven by a squeezed vacuum reservoir in a 1D waveguide; the second presents the general form of the steady-state solutions of the master equation in the collective state representation for the two giant atoms.

II. THE SYSTEM OF A TWO-LEVEL GIANT ATOM DRIVEN BY A SQUEEZED VACUUM RESERVOIR IN A 1D WAVEGUIDE

We begin by considering a single giant atom coupled to the fields in a 1D waveguide at $\mathcal{P}$ separated coupling points, where the waveguide is driven by a squeezed vacuum reservoir, as shown in Fig. 1(a). In the rotating-wave approximation (RWA), the system Hamiltonian reads ($\hbar = 1$)

$$H_1 = \omega_0\sigma_+\sigma_- + \int_{-\infty}^{\infty} dk\omega_k a_k^\dagger a_k + \sum_{n=1}^{\mathcal{P}}\int_{-\infty}^{\infty}\frac{dk}{\sqrt{2\pi}}(g_k a_k\sigma_+ e^{ikx_n} + \text{H.c.}), \tag{1}$$

where $\sigma_+ = |e\rangle\langle g|$ ($\sigma_- = |g\rangle\langle e|$) is the raising (lowering) operator of the giant atom, with transition frequency ω_0, and a_k ($a_k^\dagger$) is the annihilation (creation) operator of the kth field mode with frequency ω_k. The superscript $\mathcal{P}$ in the summation symbol represents the total number of the coupling points. The coordinate of the coupling points denotes x_n, with the same coupling strength g_k.

To describe the dynamics of the giant atom, we trace out the field modes of the waveguide and derive the quantum master equation of the atom. For the case of the waveguide in ordinary vacuum, the quantum master equation of giant atoms can be derived by using the standard techniques [59] or the SLH formalism [60–62]. However, here we consider that the waveguide is in the squeezed vacuum. The initial state of the waveguide is $\rho_w(0) = \prod_k S_k|0_k\rangle\langle 0_k|S_k^\dagger$, where $S_k(\xi) = \exp[(re^{-i\phi}a_{k_0+k}a_{k_0-k} - re^{i\phi}a_{k_0+k}^\dagger a_{k_0-k}^\dagger)]$ is the squeezed operator, with r and ϕ being the squeezing strength and squeezing angle, respectively. For simplicity, we assume that the center frequency of the squeezing field is resonant with the atomic transition frequency ω_0. In the case of ω_0 being far away from the cutoff frequency of the waveguide, the dispersion relation can be linearized as $\omega_k \approx \omega_0 + (k - k_0)\upsilon_g$, with k_0 (υ_g) being the wave vector (group velocity) of the field at frequency ω_0. The correlation functions for the squeezed vacuum are [63]

$$\begin{aligned}
\langle a_k\rangle &= \langle a_k^\dagger\rangle = 0,\\
\langle a_k^\dagger a_{k'}\rangle &= \sinh^2(r)\delta_{kk'},\\
\langle a_k a_{k'}^\dagger\rangle &= \cosh^2(r)\delta_{kk'},\\
\langle a_k a_{k'}\rangle &= -e^{i\phi}\sinh(r)\cosh(r)\delta_{k',2k_0-k},\\
\langle a_k^\dagger a_{k'}^\dagger\rangle &= -e^{-i\phi}\sinh(r)\cosh(r)\delta_{k',2k_0-k}.
\end{aligned} \tag{2}$$

The master equation of the giant atom is obtained by taking the collision-model method [24,58] within the weak-coupling regime and under the Markov approximation, where the coupling strength is treated as k independent (see Appendix A for the details). In the presence of the squeezed vacuum reservoir, the master equation for a two-level giant atom is given by

$$\dot\rho = -i[\Delta\sigma_+\sigma_-, \rho] + \Gamma^{(N)}\{(N+1)D_{\sigma_-,\sigma_+}[\rho] + ND_{\sigma_+,\sigma_-}[\rho]\} + \Gamma^{(M)}(M\sigma_+\rho\sigma_+ + M^*\sigma_-\rho\sigma_-). \tag{3}$$

It can be seen that the first two terms in Eq. (3) have the same form as in the thermal reservoir, and the last term arises from the squeezed reservoir, where $M = e^{-i\phi}\sinh(r)\cosh(r)$ and $N = \sinh^2(r)$. In Eq. (3) we introduce the

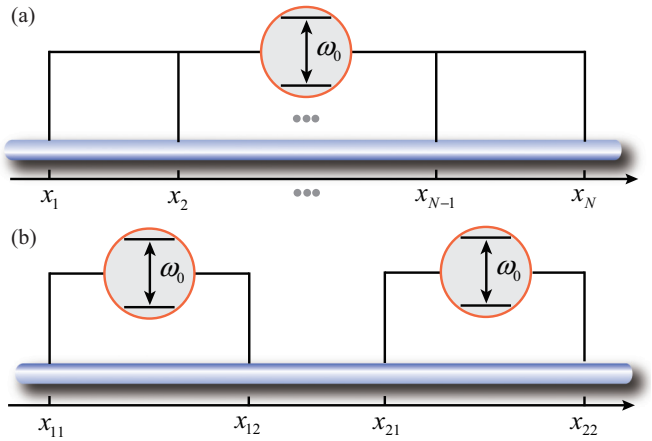

FIG. 1. (a) Schematic of a two-level giant atom coupled to a one-dimensional (1D) waveguide at multiple separated points. (b) Schematic of two giant atoms coupled to a common waveguide, where each giant atom has two separated coupling points. In both setups, the waveguide is driven by a broadband squeezed vacuum reservoir.

notation $D_{o,o^\dagger}[\rho] = o\rho o^\dagger - (o^\dagger o\rho + \rho o^\dagger o)/2$ for the Lindblad superoperators [64]. The frequency shift induced by the waveguide is given by $\Delta = \Gamma \sum_{n=1}^{\mathcal{P}-1} \sum_{m=n+1}^{\mathcal{P}} \sin[k_0(x_m - x_n)]$, and the effective decay rates are $\Gamma^{(N)} = \Gamma \sum_{m,n=1}^{\mathcal{P}} \cos[k_0(x_m - x_n)]$ and $\Gamma^{(M)} = \Gamma \sum_{m,n=1}^{\mathcal{P}} \cos[k_0(x_m + x_n)]$. Here $\Gamma = 2g^2/\upsilon_g$ is the atomic spontaneous rate. These expressions show that Δ and $\Gamma^{(N)}$ depend on the relative distances of the coupling points, while $\Gamma^{(M)}$ depends on the choice of the coordinate origin for the coupling points of the giant atom. For simplicity, we assume that the distances between neighboring points are equal. Therefore, we introduce $\theta_0 = k_0(x_{n+1} - x_n)$ to represent the phase of photons propagating between adjacent coupling points in the waveguide, and $\theta_c = k_0(x_1 + x_{\mathcal{P}})/2$ to represent the phase of the center of mass, with x_1 and $x_{\mathcal{P}}$ being the coordinates of the leftmost and rightmost coupling points of the giant atom, respectively. The physical meaning of such dependence can be explained by the fact that squeezed vacuum is not vacuum but generated by a coherent light source [54,65]. Note that the dependence of $\Gamma^{(M)}$ on θ_c is absent in a small atom. Hereafter, we refer to θ_0 and θ_c the propagating phase and the "center-of-mass phase," respectively. For the case of $\mathcal{P}$ coupling points, the relation $k_0 x_n = \theta_c + [n - (\mathcal{P}+1)/2]\theta_0$ holds. Consequently, the characteristic parameters for the master equation (3) are given by

$$\begin{aligned}
\Delta &= \Gamma \sum_{n=1}^{\mathcal{P}} (\mathcal{P} - n)\sin(n\theta_0),\\
\Gamma^{(N)} &= \Gamma \sum_{m,n=1}^{\mathcal{P}} \cos[(m-n)\theta_0],\\
\Gamma^{(M)} &= \Gamma \sum_{m,n=1}^{\mathcal{P}} \cos[2\theta_c + (m-n)\theta_0].
\end{aligned} \tag{4}$$

The dephasing dynamics of a giant atom driven by the squeezed vacuum reservoir can be seen from the time evolution of the Pauli operators. Using the master equation (3), we obtain the following Bloch equations

$$\begin{aligned}
\langle \dot{\sigma}_x \rangle &= -\Gamma_x \langle \sigma_x \rangle + \Gamma_{xy} \langle \sigma_y \rangle,\\
\langle \dot{\sigma}_y \rangle &= \Gamma_{yx} \langle \sigma_x \rangle - \Gamma_y \langle \sigma_y \rangle,\\
\langle \dot{\sigma}_z \rangle &= -\Gamma_z \langle \sigma_z \rangle - \Gamma^{(N)},
\end{aligned} \tag{5}$$

where the decay rates of $\langle \sigma_x \rangle$, $\langle \sigma_y \rangle$, and $\langle \sigma_z \rangle$ are, respectively, defined as $\Gamma_x = \Gamma^{(N)}(N + 1/2) - \Gamma^{(M)}|M|\cos\phi$, $\Gamma_y = \Gamma^{(N)}(N + 1/2) + \Gamma^{(M)}|M|\cos\phi$, and $\Gamma_z = \Gamma^{(N)}(2N + 1)$. The exchanging rates between $\langle \sigma_x \rangle$ and $\langle \sigma_y \rangle$ are defined as $\Gamma_{xy} = \Gamma^{(M)}|M|\sin\phi - \Delta$ and $\Gamma_{yx} = \Gamma^{(M)}|M|\sin\phi + \Delta$, which arise from the squeezing angle ϕ and the frequency shift Δ.

When there is only a single coupling point, Eq. (5) can reduce to the results of a small atom in the squeezed vacuum reservoir [49,66]. Considering the squeezing angle $\phi = \pi$, we have $\Delta = \Gamma_{xy} = \Gamma_{yx} = 0$, $\Gamma^{(N)} = \Gamma^{(M)} = \Gamma$, $\Gamma_{x,y} = \Gamma(N \pm |M| + 1/2)$, and $\Gamma_z = \Gamma(2N + 1)$. In the case of the squeezing strength $r = 0$, i.e., $|M| = 0$, $\langle \sigma_x \rangle$ and $\langle \sigma_y \rangle$ decay with the same rate $\Gamma_x = \Gamma_y = \Gamma$. However, when r is sufficiently large, we have $\Gamma_x = N + |M| + 1/2 \to 2N + 1$ and $\Gamma_y = N - |M| + 1/2 \to 1/8N$, indicating that the decays of $\langle \sigma_x \rangle$ and $\langle \sigma_y \rangle$ are enhanced and suppressed, respectively. In the long-time limit, we have $\langle \sigma_x \rangle \to 0$ and $\langle \sigma_z \rangle \to -1/(2N + 1)$, which means that the steady-state population of the small atom depends on only the squeezing parameter.

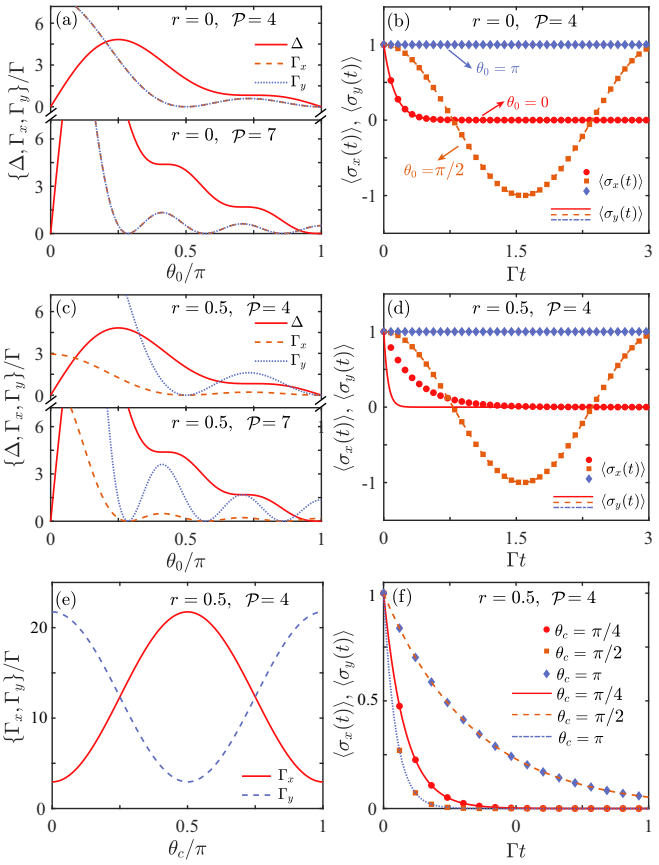

FIG. 2. (a), (c) Frequency shift Δ, decay rates Γ_x and Γ_y as functions of the propagating phase θ_0 at different squeezing strength r and coupling points $\mathcal{P}$. (b), (d) Dephasing dynamics of the giant atom at different squeezing strength. In panels (a)–(d), the center-of-mass phase takes $\theta_c = 2\pi$. (e) Decay rates Γ_x and Γ_y as functions of θ_c. (f) Dephasing dynamics of the giant atom at different values of θ_c. In panels (e) and (f), the propagating phase takes $\theta_0 = 2\pi$.

For the giant-atom case, the decay rates and the exchanging rates at $\phi = \pi$ become $\Gamma_{x,y} = \Gamma^{(N)}(N + 1/2) \pm \Gamma^{(M)}|M|$, $\Gamma_z = \Gamma^{(N)}(2N + 1)$ and $\Gamma_{xy} = -\Gamma_{yx} = -\Delta$, respectively. To see the influence of θ_0 and r on the dephasing dynamics, we first fix $\theta_c = 2\pi$. In Figs. 2(a) and 2(c), we plot the frequency shift Δ and the decay rates $\Gamma_{x,y}$ as a function of θ_0 when the squeezing strength takes $r = 0$ and $r = 0.5$, respectively, with both considering the coupling points $\mathcal{P} = 2$ and 4. We find that Δ, Γ_x, and Γ_y are periodically modulated by θ_0 with a period of 2π. Meanwhile, an increase in the number of coupling points makes Δ and $\Gamma_{x,y}$ more sensitive to θ_0. When $r = 0$, the decay rates Γ_x and Γ_y have the same dependence on θ_0 regardless of the number of the coupling points, while when $r = 0.5$, Γ_x and Γ_y exhibit different features with respect to θ_0. The time evolutions of $\langle \sigma_x(t) \rangle$ and $\langle \sigma_x(t) \rangle$ with $\mathcal{P} = 4$ are shown in Figs. 2(b) and 2(d), respectively. When

$r = 0$, $\langle\sigma_x(t)\rangle$ and $\langle\sigma_y(t)\rangle$ have the same evolution. For $\theta_0 = 0$, they exhibit the exponential decay process, which is similar to the small-atom case. For $\theta_0 = \pi/2$, the time evolution is characterized by the Rabi oscillation with frequency Δ. For $\theta_0 = \pi$, we obtain $\Delta = \Gamma_x = \Gamma_y = 0$ due to the destructive quantum interference effect induced by the multiple coupling points, and hence the giant atom is decoupled from the waveguide. When $r \neq 0$, $\langle\sigma_y(t)\rangle$ decays faster than $\langle\sigma_x(t)\rangle$. Note that although the evolution of $\langle\sigma_z(t)\rangle$ (not shown) is modulated by the coupling points $\mathcal{P}$, its steady-state value is independent of $\mathcal{P}$ and depends on only the squeezing strength.

Figure 2(e) shows the dependence of the dephasing rates of the giant atom on the center-of-mass phase θ_c, with fixed values of $\theta_0 = 2\pi$ and $\mathcal{P} = 4$. From Fig. 2(e) it is found that the dephasing rates also vary periodically as θ_c changes, but with a period of π. In the region $\theta_c \in [0, \pi/4) \bigcup (3\pi/4, \pi]$, $\langle\sigma_y(t)\rangle$ decays faster than $\langle\sigma_x(t)\rangle$, while in the region $\theta_c \in (\pi/4, 3\pi/4)$, $\langle\sigma_x(t)\rangle$ decays faster than $\langle\sigma_y(t)\rangle$. In particular, when $\theta_c = \pi/4$ or $3\pi/4$, $\langle\sigma_x(t)\rangle$ and $\langle\sigma_y(t)\rangle$ have the same time evolution. In Fig. 2(f), we plot the time evolution of $\langle\sigma_x(t)\rangle$ and $\langle\sigma_y(t)\rangle$ at $\theta_c = \pi/4, \pi/2$, and π, which confirms the analyses in Fig. 2(e).

III. THE SYSTEM OF TWO GIANT ATOMS DRIVEN BY A SQUEEZED VACUUM RESERVOIR IN A 1D WAVEGUIDE

Now we consider the case where two giant atoms are coupled to a common 1D waveguide, as shown in Fig. 1(b). Each giant atom interacts with the fields in the waveguide at two separated coupling points. The Hamiltonian of the total system reads ($\hbar = 1$)

$$H_2 = \omega_0(\sigma_1^+\sigma_1^- + \sigma_2^+\sigma_2^-) + \int_{-\infty}^{\infty} dk\omega_k a_k^\dagger a_k + \sum_{m,n=1,2}\int_{-\infty}^{\infty}\frac{dk}{\sqrt{2\pi}}(g_k a_k \sigma_m^+ e^{ikx_{mn}} + \text{H.c.}), \quad (6)$$

where σ_m^+ (σ_m^-) is the raising (lowering) operator of giant atom m, with transition frequency ω_0; a_k ($a_k^\dagger$) is the annihilation (creation) operator of the kth field mode with frequency ω_k; and x_{mn} is the position of the nth coupling point of atom m, with the same coupling strength g_k.

By tracing out the field modes in the waveguide, the quantum master equation of the two giant atoms driven by a squeezed vacuum reservoir is given by (see Appendix A)

$$\dot{\rho} = -i[H_{\text{eff}}, \rho] + \sum_{s,s'=1,2}\Gamma_{ss'}^{(N)}\{(N+1)D_{\sigma_s^-,\sigma_{s'}^+}[\rho] + ND_{\sigma_s^+,\sigma_{s'}^-}[\rho]\} + \sum_{s,s'=1,2}\Gamma_{ss'}^{(M)}\{MD_{\sigma_s^+,\sigma_{s'}^+}[\rho] + M^*D_{\sigma_s^-,\sigma_{s'}^-}[\rho]\}. \quad (7)$$

Here the first line of Eq. (7) is the coherent dynamics induced by the waveguide, with the effective Hamiltonian

$$H_{\text{eff}} = \sum_{s=1,2}\delta\omega_s\sigma_s^+\sigma_s^- + (g\sigma_1^-\sigma_2^+ + \text{H.c.}), \quad (8)$$

where $\delta\omega_s = \Gamma\sin[k_0(x_{s2} - x_{s1})]$ is the frequency shift of giant atom m and $g = \Gamma\sum_{s,s'=1,2}\sin[k_0(x_{2s} - x_{1s'})]/2$ is the dipole-dipole interaction strength between the giant atoms. The second and third lines in Eq. (7) represent the incoherent decay and squeezing with rates $\Gamma_{ss'}^{(N)} = \Gamma\sum_{m,n=1,2}\cos[k_0(x_{sm} - x_{s'n})]$ and $\Gamma_{ss'}^{(M)} = \Gamma\sum_{m,n=1,2}\cos[k_0(x_{sm} + x_{s'n})]$, respectively. Therefore, the waveguide driven by the squeezed vacuum reservoir can not only induce the frequency shift, individual decay, individual squeezing of each giant atom (for $s = s'$), but also mediate the coherent dipole-dipole interaction, collective decay, and collective squeezing (for $s \neq s'$). From these expressions we see that $\delta\omega_s$, g, and $\Gamma_{ss'}^{(N)}$ depend on the coupling-point distance. This behavior is consistent with the results of two giant atoms coupled to a 1D waveguide in ordinary vacuum [23]. However, we find that $\Gamma_{ss'}^{(M)}$ depends on the choice of the giant atom's center-of-mass coordinate. Since the collective squeezing term in Eq. (7) allows the two-photon process, it provides us an additional mechanism to control the dynamics of the two giant atoms.

Similar to the single-giant-atom case, we assume that the distances of neighboring coupling points are equal with corresponding photon-propagating phase $\theta_0 = k_0(x_{12} - x_{11}) = k_0(x_{21} - x_{12}) = k_0(x_{22} - x_{21})$. In addition, we place the center-of-mass coordinate at the midpoint between the two giant atoms, defining the center-of-mass phase as $\theta_c = k_0(x_{12} + x_{21})/2$. The dependence of the characteristic parameters $\delta\omega_s$, g, $\Gamma_{ss'}^{(N)}$, and $\Gamma_{ss'}^{(M)}$ on the phases θ_0 and θ_c is given by

$$\begin{aligned}
\delta\omega &= \Gamma\sin\theta_0,\\
g &= \frac{\Gamma}{2}[\sin\theta_0 + 2\sin(2\theta_0) + \sin(3\theta_0)],\\
\Gamma_{11}^{(N)} &= 2\Gamma(1 + \cos\theta_0),\\
\Gamma_{12}^{(N)} &= \Gamma[\cos\theta_0 + 2\cos(2\theta_0) + \cos(3\theta_0)],\\
\Gamma_{11}^{(M)} &= \Gamma\{\cos(2\theta_c - \theta_0) + 2\cos[2(\theta_c - \theta_0)] + \cos(2\theta_c - 3\theta_0)\},\\
\Gamma_{22}^{(M)} &= \Gamma\{\cos(2\theta_c + \theta_0) + 2\cos[2(\theta_c + \theta_0)] + \cos(2\theta_c + 3\theta_0)\},\\
\Gamma_{12}^{(M)} &= \Gamma\{\cos(2\theta_c - \theta_0) + 2\cos(2\theta_c) + \cos(2\theta_c + \theta_0)\}. \quad (9)
\end{aligned}$$

Here these parameters satisfy $\delta\omega = \delta\omega_1 = \delta\omega_2$, $\Gamma_{11}^{(N)} = \Gamma_{22}^{(N)}$, $\Gamma_{12}^{(N)} = \Gamma_{21}^{(N)}$, and $\Gamma_{12}^{(M)} = \Gamma_{21}^{(M)}$.

To understand the individual influence of phases θ_0 and θ_c on the characteristic parameters in Eq. (9), we fix one phase while varying the other. Figure 3(a) plots the dependence of θ_0 on the characteristic parameters at fixed $\theta_c = 2\pi$. It shows that all these parameters are periodically modulated by θ_0. Therefore, the controllable dynamics of the two giant atoms in the squeezed vacuum reservoir is accessible via manipulating θ_0. When $\theta_c = 2\pi$, the decay and squeezing rates satisfy $\Gamma_{11/22}^{(N)} = \Gamma_{12}^{(M)}$ and $\Gamma_{11/22}^{(M)} = \Gamma_{12}^{(N)}$, as shown by the purple dot-dashed and blue dotted lines in Fig. 3(a). Since $\delta\omega$, g, $\Gamma_{11/22}^{(N)}$, and $\Gamma_{12}^{(N)}$ are independent of θ_c, we plot only the squeezing rates $\Gamma_{11/22}^{(M)}$ and $\Gamma_{12}^{(M)}$ as a function of θ_c in Fig. 3(b), with fixed $\theta_0 = \pi/2$ and 2π. As seen in Fig. 3(b), $\Gamma_{11/22}^{(M)}$ and $\Gamma_{12}^{(M)}$ vary periodically with a period of π as θ_c changes. For $\theta_0 = 2\pi$,

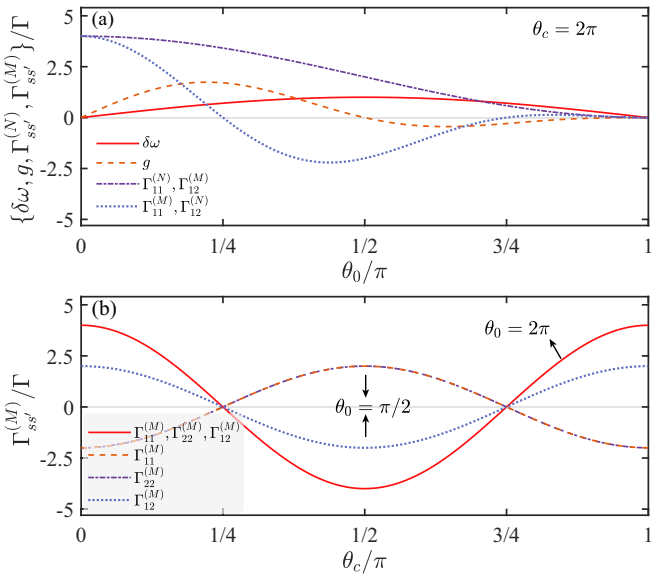

FIG. 3. (a) Characteristic parameters of the quantum master equation (7) as a function of the photon-propagating phase θ_0 with the center-of-mass phase fixed at $\theta_c = 2\pi$. (b) Characteristic parameters as a function of θ_c with propagating phase fixed at $\theta_0 = 2\pi$ and π. In panels (a) and (b), each giant atom is coupled to the waveguide at two separate coupling points.

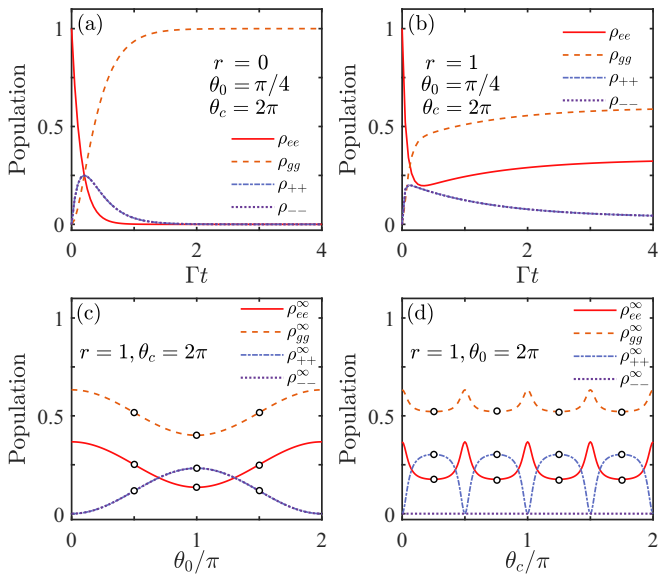

FIG. 4. Time evolution of the population for the two giant atoms in (a) the absence and (b) the presence of the squeezed vacuum reservoir, with $\theta_0 = \pi/4$ and $\theta_c = 2\pi$. Steady-state population as a function of the scaled phases: (c) θ_0/π and (d) θ_c/π, with $\theta_c = 2\pi$ and $\theta_0 = 2\pi$, respectively. In all panels, the atomic initial state is in $|\psi\rangle = |ee\rangle$.

the squeezing rates follow the same dependence on θ_c. For $\theta_0 = \pi/2$, the absolute values of the squeezing rates become small except for $\theta_c = \pi/4$ and $3\pi/4$. In particular, the rate $\Gamma_{12}^{(M)}$ varies in the opposite trend to $\Gamma_{11}^{(M)}$ and $\Gamma_{22}^{(M)}$ as θ_c changes.

A. Evolution and steady-state behavior of population of two giant atoms

In the two-giant-atom case, the dynamics of giant atoms can exhibit richer behaviors due to the waveguide-mediated dipole-dipole interaction, collective decay, and collective squeezing. To better understand the atomic dynamics, we work in the collective state representation of the two giant atoms using the basis $\{|ee\rangle, |+\rangle, |-\rangle, |gg\rangle\}$, where $|\pm\rangle = (|eg\rangle \pm |ge\rangle)/\sqrt{2}$. In this basis the quantum master equation (7) can be written as

$$
\begin{aligned}
\dot{\rho}_{ee} &= -2(N+1)\Gamma_s\rho_{ee} + N\Gamma_+\rho_{++} + N\Gamma_-\rho_{--} - M\gamma_c\rho_u,\\
\dot{\rho}_{gg} &= -2N\Gamma_s\rho_{gg} + (N+1)\Gamma_+\rho_{++} + (N+1)\Gamma_-\rho_{--}\\
&\quad - M\gamma_c\rho_u,\\
\dot{\rho}_{++} &= -(2N+1)\Gamma_+\rho_{++} + (N+1)\Gamma_+\rho_{ee} + N\Gamma_+\rho_{gg}\\
&\quad + M\gamma_+\rho_u,\\
\dot{\rho}_{--} &= -(2N+1)\Gamma_-\rho_{--} + (N+1)\Gamma_-\rho_{ee} + N\Gamma_-\rho_{gg}\\
&\quad + M\gamma_-\rho_u,\\
\dot{\rho}_u &= -2i\delta\omega\rho_v - (2N+1)\Gamma_s\rho_u + 2M\gamma_+\rho_{++} + 2M\gamma_-\rho_{--}\\
&\quad - 2M\gamma_c(\rho_{ee} + \rho_{gg}),\\
\dot{\rho}_v &= -2i\delta\omega\rho_u - (2N+1)\Gamma_s\rho_v\\
&\quad + M(\gamma_{11} - \gamma_{22})(\rho_{+-} - \rho_{-+}),\\
\dot{\rho}_{+-} &= -[2ig + (2N+1)\Gamma_s]\rho_{+-} + \tfrac{1}{2}M(\gamma_{11} - \gamma_{22})\rho_v,\\
\dot{\rho}_{-+} &= [2ig - (2N+1)\Gamma_s]\rho_{-+} - \tfrac{1}{2}M(\gamma_{11} - \gamma_{22})\rho_v. \qquad (10)
\end{aligned}
$$

Here we define $\rho_{ee} = \langle ee|\rho|ee\rangle$, $\rho_{gg} = \langle gg|\rho|gg\rangle$, $\rho_{\pm\pm} = \langle\pm|\rho|\pm\rangle$, $\rho_u = \rho_{eegg} + \rho_{ggee}$, and $\rho_v = \rho_{eegg} - \rho_{ggee}$, with $\rho_{eegg} = \langle ee|\rho|gg\rangle$ and $\rho_{ggee} = \langle gg|\rho|ee\rangle$. For convenience, in deriving Eq. (10), we introduce $\Gamma_s = \Gamma_{ss}^{(N)}$, $\Gamma_c = \Gamma_{12}^{(N)}$, $\gamma_{ss} = \Gamma_{ss}^{(M)}$, $\gamma_c = \Gamma_{12}^{(M)}$, $\Gamma_\pm = \Gamma_s \pm \Gamma_c$, and $\gamma_\pm = \gamma_c \pm (\gamma_{11} + \gamma_{22})/2$ for $s = 1, 2$.

Via numerically solving the equations of motion for the density matrix elements in Eq. (10) under the given initial condition, we show the population dynamics of the two giant atoms in Figs. 4(a) and 4(b) when the squeezing strength takes $r = 0$ and $r = 1$, respectively. The two giant atoms are assumed to be initially in the state $|\psi\rangle = |ee\rangle$. When there is no squeezing, as shown in Fig. 4(a), the populations ρ_{++}, ρ_{--}, and ρ_{gg} begin to increase at $t > 0$ due to the spontaneous emission process. In the long-time limit, all populations decay to the ground state $|gg\rangle$. When the squeezing strength $r \neq 0$, as shown in Fig. 4(b), the dynamics of $\rho_{\pm\pm}$ are similar to that when $r = 0$. However, ρ_{ee} shows a slight increase after a period of decay, eventually reaching a nonzero steady-state value. This behavior arises because the squeezed vacuum reservoir allows the transition between the ground state $|gg\rangle$ and the excited state $|ee\rangle$, as shown by the term $-M\gamma_c\rho_u$ in the first two equations of Eq. (10), and hence the two-photon process appears in this system. In the long-time limit, the population in state $|ee\rangle$ approaches its steady-state value. We will see how this feature results in the generation of remote stationary entanglement between the two giant atoms.

Figures 4(c) and 4(d) display the steady-state populations as functions of θ_0 and θ_c, respectively. In both cases the steady-state populations ρ_{gg}^∞ and ρ_{ee}^∞ differ in magnitude, but their overall trends follow the same envelope, as shown by the red solid and orange dashed lines in Figs. 4(c) and 4(d).

The periodic dependence on θ_0 and θ_c is 2π and $\pi/2$, respectively. Note that for the small-atom scheme, the steady-state populations depends on only the phase θ_c [54]. In addition, we find that the populations ρ_{++}^{∞} and ρ_{--}^{∞} show the same dependence on θ_0 in Fig. 4(c) except at $\theta_0 = \pi/2$, π, and $3\pi/2$. These points are marked by the black circles and will be explained later. In Fig. 4(d), ρ_{++}^{∞} exhibits periodic oscillations with respect to θ_c, while ρ_{--}^{∞} stays its initial value. This is different from the behavior of $\rho_{\pm\pm}^{\infty}$ in the long-time limit in Fig. 4(b). To understand these features, we analytically solve the steady-state solutions by setting the time derivatives on the left-hand side of Eq. (10) to be zero. In Appendix B we present the general form of the steady-state solutions, which depend on both θ_0 and θ_c. However, these solutions take on complicated forms. To examine the individual effects of quantum interference and squeezing, we consider two specific cases: fixing $\theta_c = 2\pi$ to study the dependence of the steady-state solutions on θ_0, and fixing $\theta_0 = 2\pi$ to study the dependence on θ_c.

We first solve the steady-state solutions of Eq. (10) as a function of θ_0, with $\theta_c = 2\pi$ fixed. For $\theta_0 \neq m\pi/2$ (where m is an integer), the steady-state solutions are given by

$$\begin{aligned}
\rho_{ee}^{\infty} &= \frac{4N^2\delta\omega^2 + N(2N+1)\Gamma_s^2}{(2N+1)^2\left(4\delta\omega^2+\Gamma_s^2\right)},\\
\rho_{\pm\pm}^{\infty} &= \frac{4N(N+1)\delta\omega^2}{(2N+1)^2\left(4\delta\omega^2+\Gamma_s^2\right)},\\
\rho_{u}^{\infty} &= \frac{-2\sqrt{N(N+1)}\Gamma_s^2}{(2N+1)\left(4\delta\omega^2+\Gamma_s^2\right)},\\
\rho_{v}^{\infty} &= \frac{4i\sqrt{N(N+1)}\delta\omega\Gamma_s}{(2N+1)^2\left(4\delta\omega^2+\Gamma_s^2\right)},\\
\rho_{\pm\mp}^{\infty} &= 0,
\end{aligned} \tag{11}$$

with the trace-preserving condition $\rho_{ee}^{\infty} + \rho_{gg}^{\infty} + \rho_{++}^{\infty} + \rho_{--}^{\infty} = 1$. Interestingly, these steady-state solutions depend on only the frequency shift $\delta\omega$ and individual decay Γ_s, and the squeezing strength r.

From Eq. (11) we see that the steady-state populations in the states $|\pm\rangle$ satisfy $\rho_{++}^{\infty} = \rho_{--}^{\infty}$, confirming the numerical results in Fig. 4(c). Meanwhile, it can be shown that the difference of the populations in $|gg\rangle$ and $|ee\rangle$ is given by $\rho_{gg}^{\infty} - \rho_{ee}^{\infty} = 1/(2N+1)$, which decreases as the squeezing strength increases. Note that in derivation of Eq. (11), we have excluded the case where the phase takes $\theta_0 = m\pi/2$, with m an integer. When $\theta_0 = (2m+1)\pi$, all characteristic parameters in Eq. (9) become zero due to the destructive interference effect. As a result, the two giant atoms are decoupled from the waveguide, and the populations maintain their initial values. When $\theta_0 = 2m\pi$, the decay rates of the states $|\pm\rangle$ are $\Gamma_+ = 8\Gamma$ and $\Gamma_- = 0$, respectively. This means that $|+\rangle$ is a bright state, while $|-\rangle$ becomes a dark state. By solving Eq. (10), the steady-state solutions are given by $\rho_{ee}^{\infty} = \frac{N(1-\rho_{--}(0))}{2N+1}$, $\rho_{--}^{\infty} = \rho_{--}(0)$, $\rho_{u}^{\infty} = -\frac{2\sqrt{N(N+1)}(1-\rho_{--}(0))}{2N+1}$, and $\rho_{++}^{\infty} = \rho_{\pm\mp}^{\infty} = \rho_{v}^{\infty} = 0$, with $\rho_{--}(0)$ the initial population in $|-\rangle$. Thus, we see that the steady-state population ρ_{++}^{∞} is zero while ρ_{--}^{∞} stays its initial value $\rho_{--}(0)$. Comparing these expressions with Eq. (11), it can be found that when $\rho_{--}(0)$ is nonzero, the steady-state values of Eq. (10) cannot be described by Eq. (11). However, if $\rho_{--}(0) = 0$, the steady-state values at $\theta_0 = 2m\pi$ can also be described by Eq. (11). On the contrary, by tuning the propagating phase to $\theta_0 = (2m+1)\pi/2$, the decays of the states $|\pm\rangle$ are $\Gamma_+ = 0$ and $\Gamma_- = 4\Gamma$, indicating that $|+\rangle$ and $|-\rangle$ correspond to the dark and bright states, respectively. In this case, the steady-state solutions of Eq. (10) at $\theta_0 = (2m+1)\pi/2$ are calculated as $\rho_{ee}^{\infty} = \frac{N(3N+1)}{7N^2+7N+2}[1-\rho_{++}(0)]$, $\rho_{++}^{\infty} = \rho_{++}(0)$, $\rho_{--}^{\infty} = \frac{N(N+1)}{7N^2+7N+2}[1-\rho_{++}(0)]$, $\rho_{u}^{\infty} = -\frac{2\sqrt{N(N+1)}(2N+1)}{7N^2+7N+2}[1-\rho_{++}(0)]$, $\rho_{v}^{\infty} = \frac{2i\sqrt{N(N+1)}}{7N^2+7N+2}[1-\rho_{++}(0)]$, and $\rho_{\pm\mp}^{\infty} = 0$, with $\rho_{++}(0)$ being the initial population in $|+\rangle$. Based on these expressions, we find that Eq. (11) is invalid for $\theta_0 = (2m+1)\pi/2$ even if there is no initial population in $|+\rangle$. Therefore, for $\theta_0 = (2m+1)\pi/2$ and $(2m+1)\pi$, the steady-state solutions of Eq. (10) cannot be described by Eq. (11). To address this, we use the black circles in Fig. 4(c) to exclude these values.

In the following, we fix $\theta_0 = 2\pi$ to see the influence of the center-of-mass phase θ_c and the squeezing strength r on the steady-state solutions of Eq. (10). As mentioned before, $|-\rangle$ is a dark state at $\theta_0 = 2\pi$. Therefore, the steady-state solutions will be affected by the initial population in $|-\rangle$. After some algebra, the steady-state solutions are given by

$$\begin{aligned}
\rho_{ee}^{\infty} &= \frac{N[N(2N+1)\tan^2(2\theta_c)+1](1-\rho_{--}(0))}{(2N+1)[1+(3N^2+3N+1)\tan^2(2\theta_c)]},\\
\rho_{++}^{\infty} &= \frac{N(N+1)(1-\rho_{--}(0))\tan^2(2\theta_c)}{1+(3N^2+3N+1)\tan^2(2\theta_c)},\\
\rho_{--}^{\infty} &= \rho_{--}(0),\\
\rho_{u}^{\infty} &= \frac{-2\sqrt{N(N+1)}(1-\rho_{--}(0))}{(2N+1)[1+(3N^2+3N+1)\tan^2(2\theta_c)]\cos(2\theta_c)},\\
\rho_{v}^{\infty} &= 0,\\
\rho_{\pm\mp}^{\infty} &= 0.
\end{aligned} \tag{12}$$

Different from the case of giant atoms coupled to the waveguide in the vacuum reservoir, Eq. (12) shows that the center-of-mass phase plays an important role in the control of the atomic steady-state behavior. Here we have the population difference $\rho_{gg}^{\infty} - \rho_{ee}^{\infty} = \frac{[(2N+1)^2\tan^2(2\theta_c)+1][1-\rho_{--}(0)]}{(2N+1)[1+(3N^2+3N+1)\tan^2(2\theta_c)]}$. It depends on both the values of r and θ_c, which is different from that in Fig. 4(c). When $\theta_c = m\pi/2$, the steady-state solutions of Eq. (10) are given by $\rho_{ee}^{\infty} = \frac{N(1-\rho_{--}(0))}{2N+1}$, $\rho_{--}^{\infty} = \rho_{--}(0)$, $\rho_{u}^{\infty} = (-1)^{m+1}\frac{2\sqrt{N(N+1)}[1-\rho_{--}(0)]}{(2N+1)}$, and $\rho_{++}^{\infty} = \rho_{v}^{\infty} = \rho_{\pm\mp}^{\infty} = 0$. From these results, we know that at $\theta_0 = 2\pi$ and $\theta_c = m\pi/2$, $|+\rangle$ is a bright state and its population decays to zero in the long-time limit, while $|-\rangle$ is a dark state. As shown in Fig. 4(d), when the two giant atoms are initially in $|\psi\rangle = |ee\rangle$, the steady-state population ρ_{--}^{∞} is zero (indicated by the purple dashed line), but it will maintain $\rho_{--}^{\infty} = 1/2$ when $|\psi\rangle = |eg\rangle$ [not shown in Fig. 4(d)]. In addition, we find that the steady-state values cannot be described by Eq. (12) when $\theta_c = (2m+1)\pi/4$. By substituting $\theta_c = (2m+1)\pi/4$ into Eq. (10), we obtain $\rho_{ee}^{\infty} = \frac{N^2[1-\rho_{--}(0)]}{3N^2+3N+1}$, $\rho_{++}^{\infty} = \frac{N(N+1)[1-\rho_{--}(0)]}{3N^2+3N+1}$, $\rho_{--}^{\infty} = \rho_{--}(0)$, and $\rho_{u}^{\infty} = \rho_{v}^{\infty} = \rho_{\pm\mp}^{\infty} = 0$. Similarly, we use the black circles in Fig. 4(d) to exclude these values.

B. Entanglement generation of two giant atoms

The creation of quantum entanglement in a noisy environment is an interesting topic in quantum computation and quantum information processing [67–69]. When considering long-distance information processing, the devices need to be spaced further apart. Waveguide QED has shown unique advantages in long-distance information processing, especially providing a good platform for the generation of remote entanglement between separated emitters. Most of previous works focus on the influence of quantum interference effects induced by emitter's coupling points or the atomic external driving fields on the entanglement generation [43–47,70–79]. Different from these works, here we explore the combined influence of quantum self-interference effect and squeezing effect on the generation of giant-atom entanglement. By tuning the system parameters, we can achieve a stationary maximally entangled state of the two giant atoms.

We first focus on the entanglement dynamics of the two giant atoms via solving the master equation (7) under given initial conditions. To quantify entanglement between two two-level atoms, we adopt the Wootters concurrence [80,81]. For a system described by a density matrix ρ, the concurrence C is defined as

$$C(t) = \max\{0, \sqrt{\lambda_1} - \sqrt{\lambda_2} - \sqrt{\lambda_3} - \sqrt{\lambda_4}\}, \tag{13}$$

where λ_i for $i = 1, 2, 3, 4$ are the eigenvalues of the matrix $R = \rho(t)(\sigma_1^y \otimes \sigma_2^y)\rho^*(t)(\sigma_1^y \otimes \sigma_2^y)$. The symbols σ_1^y and σ_2^y are the Pauli matrices of atoms 1 and 2, respectively, and $\rho^*(t)$ is the conjugate of $\rho(t)$. For maximally entangled atoms $C(t) = 1$, while $C(t) = 0$ for unentangled atoms. When the density matrix takes an "X" form, with nonzero elements only along the main diagonal and antidiagonal, the concurrence in Eq. (13) can be expressed as [82,83]

$$C(t) = 2\max[0, |\rho_{egge}| - \sqrt{\rho_{ee}\rho_{gg}}, |\rho_{eegg}| - \sqrt{\rho_{egeg}\rho_{gege}}], \tag{14}$$

where ρ_{egge} and ρ_{eegg} correspond to single- and two-photon coherence terms, respectively. It can be found that the steady-state density matrix of the two atoms takes the "X" form by substituting Eqs. (11) and (12) into $\rho_{\pm\pm}^{\infty} = \frac{1}{2}(\rho_{egeg}^{\infty} \pm \rho_{egge}^{\infty} \pm \rho_{geeg}^{\infty} + \rho_{gege}^{\infty})$, $\rho_{\pm\mp}^{\infty} = \frac{1}{2}(\rho_{egeg}^{\infty} \mp \rho_{egge}^{\infty} \pm \rho_{geeg}^{\infty} - \rho_{gege}^{\infty})$, $\rho_u^{\infty} = \rho_{eegg}^{\infty} + \rho_{ggee}^{\infty}$, and $\rho_v^{\infty} = \rho_{eegg}^{\infty} - \rho_{ggee}^{\infty}$. In this case, we are able to derive an analytical expression for the steady-state concurrence under certain conditions.

In Fig. 5 we plot the time evolution of the concurrence of the two giant atoms with different atomic initial states. The center-of-mass phase is fixed at $\theta_c = 2\pi$ and the propagating phase takes $\theta_0 = \pi/4$, $\pi/2$, π, and 2π in each panel. Except for $\theta_0 = \pi$, the concurrence evolves over time and approaches its steady-state value in the long-time limit. This is because the two giant atoms are decoupled from the waveguide when $\theta_0 = \pi$, as shown by the blue dot-dashed line. Therefore, for the initial separated states $|gg\rangle$, $|ee\rangle$, and $|eg\rangle$, the atomic entanglement cannot be generated through the spontaneous emission and two-photon processes, but the concurrence will maintain its initial value 1 for a maximal entangled state $(|ee\rangle + |gg\rangle)/\sqrt{2}$. When $\theta_0 = \pi/4$, $\pi/2$, and 2π, the concurrences at initial states $|gg\rangle$, $|ee\rangle$, and $(|ee\rangle + |gg\rangle)/\sqrt{2}$ evolve into the same steady state. Compared to the small-atom case

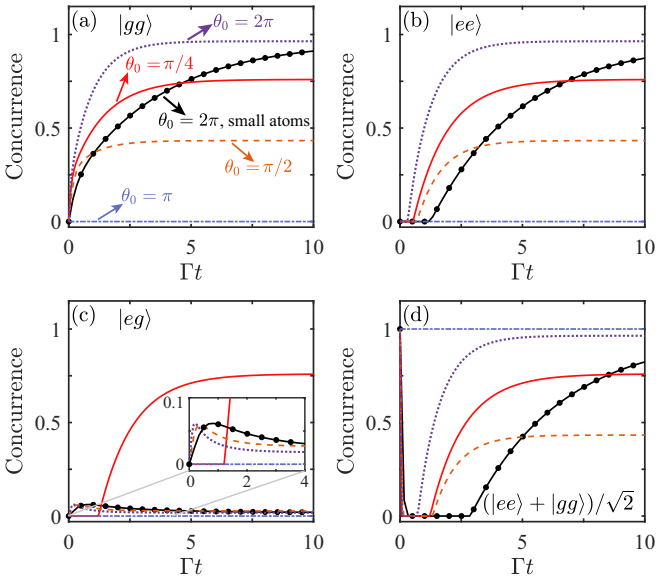

FIG. 5. Time evolution of the concurrence of the two giant atoms initially in different states. In each panel, we take typical values of the propagating phase: $\theta_0 = \pi/4$, $\pi/2$, π, and 2π. The black line with dots corresponds to the concurrence of two small atoms at $\theta_0 = 2\pi$. Other parameters are $r = 1$ and $\theta_c = 2\pi$.

(marked by the black line with dots), the concurrence of the two giant atoms reaches its steady state faster. This is due to the significant enhancement of the effective decay rate and squeezing rate caused by the constructive interference. For different values of θ_0, the concurrence of the small atoms reaches the same steady-state value. Among all the values of θ_0, the concurrence of the small atoms reaches steady state the faster at $\theta_0 = 2\pi$. Thus, Fig. 5 shows only the case for $\theta_0 = 2\pi$. However, even at this value, the small-atom concurrence reaches its steady state more slowly than that of giant atoms. For the case of the single-excitation initial state $|eg\rangle$, there exists initial population $\rho_{++}(0)$ $[\rho_{--}(0)]$. Since $|+\rangle$ $(|-\rangle)$ is a dark state at $\theta_0 = (2m+1)\pi$ $(2m\pi)$, its steady-state population stays at $\rho_{++}(0)$ $[\rho_{--}(0)]$. This causes different behaviors of the concurrence, as shown in the inset of Fig. 5(c).

If there is no initial population in the states $|\pm\rangle$, i.e., $\rho_{\pm\pm}(0) = 0$, the steady-state concurrence for $\theta_0 \neq (2m+1)\pi/2$ is given by

$$C_{\infty} = \max\left\{0, \frac{2\sqrt{N(N+1)}|(2N+1)\Gamma_s^2 - 2i\delta\omega\Gamma_s|}{(2N+1)^2(4\delta\omega^2 + \Gamma_s^2)} - \frac{8N(N+1)\delta\omega^2}{(2N+1)^2(4\delta\omega^2 + \Gamma_s^2)}\right\}. \tag{15}$$

Equation (15) shows that we can obtain the stationary entanglement on demand by tuning the values of θ_0 and r. This is different from the small-atom case, where the steady-state concurrence is independent of θ_0. If we take $\delta\omega = 0$, the steady-state concurrence reduces to the result in [54], which depends only on the squeezing strength. For $\theta_0 = (2m+1)\pi/2$ and $\theta_c = 2\pi$, the steady-state populations are obtained as $\rho_{ee}^{\infty} = \frac{N(3N+1)}{7N^2+7N+2}$, $\rho_{--}^{\infty} = \frac{N(N+1)}{7N^2+7N+2}$, $\rho_u^{\infty} = -\frac{2\sqrt{N(N+1)}(2N+1)}{7N^2+7N+2}$, $\rho_v^{\infty} = \frac{2i\sqrt{N(N+1)}}{7N^2+7N+2}$, and $\rho_{++}^{\infty} = \rho_{\pm\mp}^{\infty} = 0$.

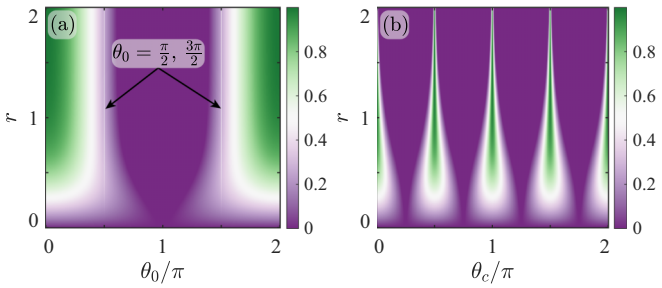

FIG. 6. Steady-state concurrence as a function of (a) θ_0 and r, (b) θ_c and r, with $\theta_c = 2\pi$ in (a) and $\theta_0 = 2\pi$ in (b).

According to these expressions, the corresponding steady-state concurrence is given by

$$C_\infty = \frac{2\sqrt{N(N+1)}\sqrt{4N^2+4N+2} - N(N+1)}{7N^2+7N+2}. \quad (16)$$

As shown by the orange dashed lines in Figs. 5(a), 5(b), and 5(d), the steady-state concurrence is lower than that for $\theta_0 = \pi/4$ and 2π. As the squeezing strength $r \to \infty$, the steady-state concurrence approaches a value of $3/7$.

The steady-state concurrences in Eqs. (15) and (16) focus on the case of zero initial population in the states $|\pm\rangle$. When the atomic initial state is in $|\psi\rangle = |eg\rangle$, we have $\rho_{\pm\pm}(0) = 1/2$. By solving Eq. (10) in the cases of $\theta_0 = 2\pi$ and $\theta_0 = \pi/2$, the steady-state concurrences are given by $C_\infty = \frac{2N+1-2\sqrt{N(N+1)}}{2(2N+1)}$ and $C_\infty = \frac{1}{2(7N^2+7N+2)}[6N^2+7N+1-2\sqrt{N(3N+1)(N+1)(3N+2)}]$, respectively. As shown in the inset of Fig. 5(c), the steady-state entanglement of both the small and giant atoms is much smaller compared to the cases shown in Figs. 5(a), 5(b), and 5(d). This indicates that when there exists initial population in the dark state $|+\rangle$ or $|-\rangle$, larger stationary atomic entanglement cannot be achieved through the spontaneous emission and two-photon decay processes.

When the propagating phase is fixed at $\theta_0 = 2\pi$, we can see the combined influence of θ_c and r on the steady-state entanglement generation. In Sec. III A we obtain specific expressions of the steady-state populations when θ_c takes $m\pi/2$ and $(2m+1)\pi/4$, respectively. For general values of θ_c, the steady-state concurrence can be obtained by calculating the population, one-photon, and two-photon coherence terms in Eq. (14). However, the detailed expression is not provided here due to its complexity. In the previous calculations, for $\theta_0 = 2\pi$ and $\theta_c = m\pi/2$, we obtained $C_\infty = \frac{2\sqrt{N(N+1)}}{2N+1}$ for $\rho_{--}(0) = 0$ and $C_\infty = \frac{2N+1-2\sqrt{N(N+1)}}{2(2N+1)}$ for $\rho_{--}(0) = 1/2$. When $\theta_c = \pi/4$, by substituting the corresponding steady-state solutions from Eq. (10), we obtain $C_\infty = 0$ for $\rho_{--}(0) = 0$ and $C_\infty = \frac{1}{2(3N^2+3N+1)}$ for $\rho_{--}(0) = 1/2$.

Figure 6(a) shows the steady-state concurrence C_∞ as a function of θ_0 and r when $\theta_c = 2\pi$. It can be observed that C_∞ is periodically modulated by θ_0, with a period of 2π. When the squeezing strength r is small, C_∞ shows little sensitivity to changes in θ_0. However, as r increases, C_∞ rises rapidly near $\theta_0 = 2m\pi$ [the green regions in Fig. 6(a)], and drops significantly when θ_0 lies within the range of $[\pi/2, 3\pi/2]$ [the purple regions in Fig. 6(a)]. Note that since the steady-state concurrence at $\theta_0 = \pi/2$ and $3\pi/2$ is given by Eq. (16) rather than Eq. (15), the changes in C_∞ are not smooth with respect to θ_0. As shown in Fig. 6(a), two distinct white lines can be observed, as indicated by the black arrows. Figure 6(b) shows the variation of C_∞ with respect to θ_c and r when $\theta_0 = 2\pi$. We see that C_∞ also exhibits periodic behavior with respect to θ_c, but has a period of $\pi/2$. Compared to the dependence of C_∞ on θ_0, C_∞ is more sensitive to changes in θ_c. As r increases, the green regions in Fig. 6(b) gradually become narrower. This indicates that C_∞ primarily appears around $\theta_0 = m\pi/2$, and even a small deviation of θ_c can lead to the steady-state entanglement to vanish. Therefore, careful control of both θ_0 and θ_c is essential for achieving the desired remote steady-state entanglement of the two giant atoms.

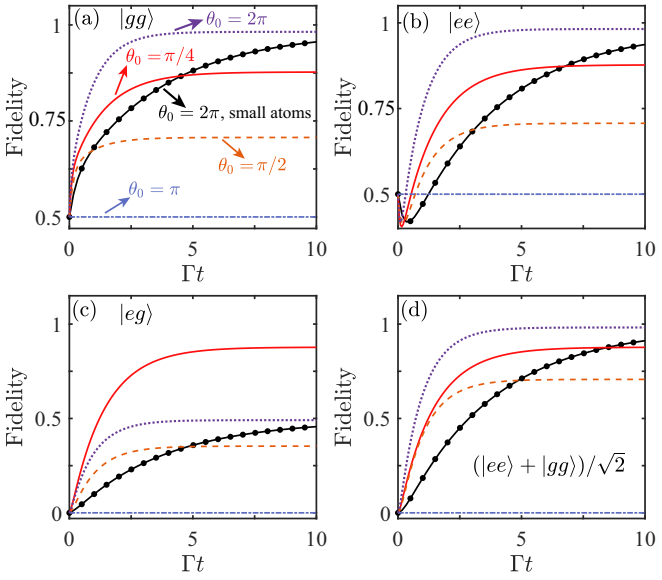

FIG. 7. Time evolution of the fidelity between the evolving state $\rho(t)$ and the target state $|\Phi\rangle = (|ee\rangle - |gg\rangle)/\sqrt{2}$ for different initial atomic states. In each panel, we take the propagating phase: $\theta_0 = \pi/4, \pi/2, \pi$, and 2π. Other parameters are $r = 1$ and $\theta_c = 2\pi$.

On the other hand, determining the specific form of the steady state is also crucial. Figure 7 shows the time evolution of the fidelity $F(t) = \sqrt{\langle\Phi|\rho(t)|\Phi\rangle}$, which measures the overlap between the atomic evolving state $\rho(t)$ and the target state $|\Phi\rangle = (|ee\rangle - |gg\rangle)/\sqrt{2}$. When $\theta_0 = \pi$, as shown by the blue dot-dashed lines, the giant atoms are decoupled from the waveguide. Thus, the fidelities in the atomic initial states $|\psi\rangle = |gg\rangle$ and $|ee\rangle$ [$|eg\rangle$ and $(|ee\rangle + |gg\rangle)/\sqrt{2}$] maintain their initial value $F(0) = 0.5$ [$F(0) = 0$]. When $\theta_0 = \pi/4$, $\pi/2$, and 2π, the steady-state values of the fidelities in the cases of $|\psi\rangle = |gg\rangle$, $|ee\rangle$, and $(|ee\rangle + |gg\rangle)/\sqrt{2}$ are identical, despite their different transient behaviors before reaching the steady state. For $|\psi\rangle = |gg\rangle$, the existence of the squeezed vacuum reservoir leads to an increase in fidelity, as shown in Fig. 7(a). However, for $|\psi\rangle = |ee\rangle$, the fidelity $F(t)$ initially decreases briefly before increasing to its steady-state value, as shown in Fig. 7(b). This behavior can be understood in terms of the population decay process. In the collective state representation, the spontaneous emission process causes the population in the state $|ee\rangle$ to decay to the states $|\pm\rangle$ and then further decay to the ground state $|gg\rangle$. At earlier times, the mixing

of these states results in a decrease in fidelity. In addition, the collective squeezing term allows the two-photon process that alters population ratio in these states. As time increases, the populations in $|\pm\rangle$ start to decay, causing the fidelity to grow. For $|\psi\rangle = |eg\rangle$ with $\theta_0 = \pi/2$ and 2π, the fidelity $F(t)$ in Fig. 7(c) is lower than that of the other three initial states. Compared to the results in Fig. 7, we find that the steady-state value of $F(t)$ almost approaches 1 when $\theta_0 = 2\pi$, as shown by the purple dashed lines in Figs. 5(a), 5(b), and 5(d). This means that the two giant atoms can approximately evolve into the target state $|\Phi\rangle = (|ee\rangle - |gg\rangle)/\sqrt{2}$. To verify this, we take $\theta_0 = 2\pi$ and $\theta_c = m\pi/2$, the steady-state solutions of Eq. (10) are given by $\rho_{ee}^{\infty} = \frac{N}{2N+1}$, $\rho_u^{\infty} = (-1)^{m+1}\frac{2\sqrt{N(N+1)}}{2N+1}$, and $\rho_{\pm\pm}^{\infty} = \rho_{\pm\mp}^{\infty} = \rho_v^{\infty} = 0$, resulting in the following entangled state:

$$|\psi_\infty\rangle = \sqrt{\frac{N}{2N+1}}|ee\rangle + (-1)^{m+1}\sqrt{\frac{N+1}{2N+1}}|gg\rangle. \tag{17}$$

In the limit $r \to \infty$, the state in Eq. (17) becomes the maximally entangled state $[|ee\rangle + (-1)^{m+1}|gg\rangle]/\sqrt{2}$. Thus, by properly controlling the squeezing strength r and these two phases, we can generate the maximally entangled state of two remote giant atoms.

IV. DISCUSSION AND CONCLUSION

We discuss the experimental feasibility of implementing giant atoms driven by a squeezed vacuum reservoir in a one-dimensional waveguide. Giant atoms have been experimentally demonstrated in several platforms, such as superconducting circuit systems [2,3,5–7] and waveguide magnon systems [84]. In addition, the community in quantum optics also propose other alternative theoretical schemes to realize giant atoms, such as synthetic dimensions [32,85], cold atoms in optical lattices [86], or Rydberg atoms in the optical regime [45]. In our scheme, we assume that the waveguide is fed by a squeezed vacuum field, which could be realized via using a Josephson parametric amplification [51,87,88] or an optical parametric down conversion [89,90]. Therefore, all these advances could provide the experimental feasibility to our proposed scheme under the current and near-future conditions.

In conclusion, we have studied the dynamics and stationary behaviors of giant atoms by considering a 1D waveguide coupled to a single and two giant atoms, respectively. In both cases, the waveguide is driven by a squeezed vacuum reservoir, which allows the giant atoms to exhibit features different from those in an ordinary vacuum reservoir. It was shown that the dephasing dynamics of single giant atom, as well as the population and entanglement evolution of two giant atoms, are jointly determined by the squeezing strength, the photon-propagating phase, and the atomic center-of-mass phase. In the single-giant-atom case, the dephasing rate can be enhanced or suppressed. In particular, by tuning the quantum self-interference effect of the giant atom, the dephasing rate can vanish, which is absent in a small atom. When extended to the two-giant-atom case, the squeezed vacuum reservoir not only induces the frequency shift, individual, and collective dissipation of the giant atoms, but also enables individual and collective squeezing. As a result, both spontaneous emission and two-photon processes coexist. Compared to small atoms, giant atoms can reach their steady-state entanglement faster. The steady-state entanglement can be adjusted by the propagating phase, which is not observed in small atoms in squeezed vacuum. It should be highlighted that when there exists a dark state in the system, any initial population in the dark state should be avoided to achieve higher entanglement. In addition, the steady-state entanglement is more sensitive to changes in the center-of-mass phase. The proper choice of these two phases can realize the maximal stationary entanglement of remote giant atoms. These results will pave the way for the constructing quantum networks and realizing quantum information processing in giant-atom waveguide-QED systems driven by squeezed vacuum fields.

ACKNOWLEDGMENTS

This work is partially financially supported by Innovation Program for Quantum Science and Technology 2023ZD0300600, Guangdong Provincial Quantum Science Strategic Initiative (No. GDZX2200001), Hong Kong Research Grant Council (RGC) under Grant No. 15213924, and National Natural Science Foundation of China under Grant No. 62173288.

APPENDIX A: DERIVATION OF THE GENERAL QUANTUM MASTER EQUATION OF GIANT ATOMS

In this Appendix, we present the derivation of the quantum master equation of giant atoms coupled to a one-dimensional waveguide driven by a squeezed vacuum field via the collisional approach [24,25,58]. The total Hamiltonian of the two-level giant atoms + field system is

$$\begin{aligned} H &= H_a + H_w + H_I, \\ H_a &= \sum_{j=1}^{P_a} \omega_0 \sigma_j^+ \sigma_j^-, \\ H_w &= \int_{-\infty}^{\infty} dk\, \omega_k a_k^\dagger a_k, \\ H_I &= \sum_{l=1}^{P_a}\sum_{j=1}^{P_j}\int_{-\infty}^{\infty} dk \frac{g_k e^{ikx_{jl}}}{\sqrt{2\pi}} a_k \sigma_j^+ + \text{H.c.}, \end{aligned} \tag{A1}$$

where H_a is the free Hamiltonian of the giant atoms, H_w is the free Hamiltonian of the waveguide with the dispersion relation ω_k, and H_I is the interaction Hamiltonian between the giant atoms and the fields in the waveguide. The upper indicies P_a and P_j of the summation symbol represent the number of giant atoms and the coupling points of giant atom j, respectively. The coordinate of the lth coupling point of atom j denotes x_{jl} with the same coupling strength g_k. For convenience, $c_k = a_{k\geqslant 0}$ and $c_k' = a_{k<0}$ are introduced to represent the right- and left-propagating field modes, respectively.

In the case of the frequency ω_0 being far from the cutoff of the dispersion, the dispersion relation for the right (left) branch around k_0 ($-k_0$) can be linearized as $\omega_k = \omega_0 + \upsilon_g(k - k_0)$ ($\omega_0 - \upsilon_g(k + k_0)$) [91,92]. Since we are interested in a narrow bandwidth in vicinity of ω_0, the range of k can be extended to $(-\infty, \infty)$. The coupling strengthes between the

giant atoms with the right- and left-propagating field modes are, respectively, assumed as $g_{k\geqslant 0} \approx g_{k_0} = g_R$ and $g_{k<0} \approx g_{-k_0} = g_L$. This approximation corresponds to the Markovian approximation [93]. By further making the variable change $(k - k_0) \to k$ $[-(k + k_0) \to k]$ and redefining the operators $c_{k-k_0} \to c_k$ $[c'_{-(k+k_0)} \to c'_k]$, the Hamiltonians H_w and H_I in the frequency domain are given by

$$\begin{aligned} H_w &= \omega_0 \int_{-\infty}^{\infty} d\omega [c^\dagger(\omega)c(\omega) + c'^\dagger(\omega)c'(\omega)] \\ &\quad - \int_{-\infty}^{\infty} d\omega\, \omega c^\dagger(\omega)c(\omega) + \int_{-\infty}^{\infty} d\omega\, \omega c'^\dagger(\omega)c'(\omega), \\ H_I &= \sum_{l=1}^{P_a}\sum_{j=1}^{P_j} \sigma_j^+ \int_{-\infty}^{\infty} d\omega \Bigg[\frac{g_R}{\sqrt{2\pi}} c(\omega) e^{i(\omega_0+\omega)\tau_{jl}} \\ &\quad + \frac{g_L}{\sqrt{2\pi}} c'(\omega) e^{-i(\omega_0+\omega)\tau_{jl}} \Bigg] + \text{H.c.} \end{aligned} \tag{A2}$$

Here $c(\omega) = c_k/\sqrt{\upsilon_g}$ and $c'(\omega) = c'_k/\sqrt{\upsilon_g}$ are the operators in the frequency domain. The parameter $\tau_{jl} = x_{jl}/\upsilon$ is defined as the propagating time of photons between coupling points. In the interaction picture with respect to $S(t) = \exp[-i(H_a + H_w)t]$, we obtain

$$\begin{aligned} H_I(t) &= S(t)^\dagger H_I S(t) \\ &= \sum_{l=1}^{P_a}\sum_{j=1}^{P_j} \Bigg[\sqrt{\gamma_R} e^{i\omega_0\tau_{jl}} \sigma_j^+ \frac{1}{\sqrt{2\pi}} \int_{-\infty}^{\infty} d\omega\, c(\omega) \\ &\quad \times e^{-i\omega(t-\tau_{jl})} + \sqrt{\gamma_L} e^{-i\omega_0\tau_{jl}} \sigma_j^+ \frac{1}{\sqrt{2\pi}} \\ &\quad \times \int_{-\infty}^{\infty} d\omega\, c'(\omega) e^{-i\omega(t+\tau_{jl})} \Bigg] + \text{H.c.} \\ &= \sum_{\alpha=1}^{\mathcal{P}} [\sqrt{\gamma_R} O_\alpha^\dagger c(t - \tau_\alpha) \\ &\quad + \sqrt{\gamma_L} O_\alpha'^\dagger c'(t + \tau_\alpha)] + \text{H.c.}, \end{aligned} \tag{A3}$$

where $\gamma_R = g_R^2/\upsilon_g$ and $\gamma_L = g_L^2/\upsilon_g$ are the atomic spontaneous emission rates induced by the right- and left-propagating modes, respectively. In the last line of Eq. (A3), we introduce the Fourier transformation $x(t) = 1/\sqrt{2\pi}\int_{-\infty}^{\infty} d\omega\, x(\omega) e^{-i\omega t}$ for $x = c$ and c', which follows the bosonic commutation rules $[x(t), x^\dagger(t')] = \delta(t - t')$, $[x(t), x(t')] = [x^\dagger(t), x^\dagger(t')] = 0$. The symbol $\alpha = 1, \cdots, \mathcal{P}$ is used to label all coupling points from left to right, i.e., $x_1 < x_2 < \cdots x_{\mathcal{P}}$. In the spirit of the collision model, the giant atoms could be regarded as a set of $\mathcal{P} = \sum_{j=1}^{P_a} P_j$ small atoms [24,25]. For each coupling point α, the lowering operators for the giant atoms are written as

$$O_\alpha = \sigma_j^- e^{-i\omega_0\tau_{jl}}, \quad O'_\alpha = \sigma_j^- e^{i\omega_0\tau_{jl}}. \tag{A4}$$

Assuming a discrete time axis $t_n = n\delta t$, with δt being the interval time of each collision, the time evolution operator is

$$U(t) = \mathcal{T} \exp\left(-i \int_0^t ds\, H_I(s)\right) = \prod_{n=1}^{[t/\delta t]} U_n(t), \tag{A5}$$

where $\mathcal{T}$ is the time-order operator and U_n is the evolution operator in the time interval $t \in [t_{n-1}, t_n]$. In the case of the time step much shorter than the characteristic interaction time, i.e., $\delta t \ll \gamma_{L/R}^{-1}$, U_n is approximated as

$$U_n \simeq I - i(\bar{V} + H_{\text{eff}})\delta t - \tfrac{1}{2}\bar{V}^2\delta t^2, \tag{A6}$$

with the average Hamiltonian and effective Hamiltonian

$$\begin{aligned} \bar{V} &= \frac{1}{\delta t}\int_{t_{n-1}}^{t_n} ds\, H_I(s), \\ H_{\text{eff}} &= \frac{i}{2\delta t}\int_{t_{n-1}}^{t_n} ds \int_{t_{n-1}}^{s} ds' [H_I(s'), H_I(s)]. \end{aligned} \tag{A7}$$

We consider the case where the propagating time of photons are negligible, i.e., $\tau_{\mathcal{P}} - \tau_1 \ll \delta t \ll \gamma_{R/L}^{-1}$. According to Eqs. (A3) and (A7), we obtain

$$\begin{aligned} \bar{V} &= \sum_{\alpha=1}^{\mathcal{P}} \Bigg[\sqrt{\frac{\gamma_R}{\delta t}} O_v^\dagger \frac{1}{\sqrt{\delta t}} \int_{t_{n-1}}^{t_n} ds\, c(s - \tau_\alpha) \\ &\quad + \sqrt{\frac{\gamma_L}{\delta t}} O_v'^\dagger \frac{1}{\sqrt{\delta t}} \int_{t_{n-1}}^{t_n} ds\, c'(s + \tau_\alpha) \Bigg] + \text{H.c.} \\ &\simeq \frac{1}{\sqrt{\delta t}} (\sqrt{\gamma_R} O^\dagger c_n + \sqrt{\gamma_L} O'^\dagger c'_n + \text{H.c.}) \end{aligned} \tag{A8}$$

and

$$\begin{aligned} H_{\text{eff}} &= i \sum_{\alpha,\alpha'}^{\mathcal{P}} \int_{t_{n-1}}^{t_n} ds \int_{t_{n-1}}^{s} ds' \gamma_R \{O_{\alpha'}^\dagger O_\alpha [c(s' - \tau_{\alpha'}), c^\dagger(s - \tau_\alpha)] \\ &\quad + \gamma_L O_{\alpha'}'^\dagger O'_\alpha [c'(s' + \tau_{\alpha'}), c'^\dagger(s + \tau_\alpha)] - \text{H.c.}\}/2\delta t \\ &\simeq \frac{i}{2} \sum_{\alpha>\alpha'}^{\mathcal{P}} (\gamma_R O_{\alpha'}^\dagger O_\alpha + \gamma_L O_\alpha'^\dagger O'_{\alpha'} - \text{H.c.}), \end{aligned} \tag{A9}$$

where we define

$$x_n = 1/\sqrt{\delta t} \int_{t_{n-1}}^{t_n} ds\, x(s), \tag{A10}$$

for $x = c, c'$ and introduce the atoms' collective operator $O = \sum_\alpha O_\alpha$.

The collision model method assumes that the field consists of a large collection of smaller identical subunits (ancillas) labeled by an integer number n [58]. Starting from an initial joint state of giant atoms and the field

$$\rho_{\text{tot}}(0) = \rho(0) \otimes \eta_1 \otimes \cdots \otimes \eta_n \otimes \cdots, \tag{A11}$$

the state $\rho_{\text{tot}}(t_n)$ at each collision becomes

$$\begin{aligned} \delta\rho_{\text{tot}}(t_n) &= \rho_{\text{tot}}(t_n) - \rho_{\text{tot}}(t_{n-1}) \\ &= U_n(t)\rho_{\text{tot}}(t_{n-1})U_n(t)^\dagger - \rho_{\text{tot}}(t_{n-1}) \\ &= -i[H_{\text{eff}} + \bar{V}, \rho_{\text{tot}}(t_{n-1})]\delta t \\ &\quad + \left(\bar{V}\rho_{\text{tot}}(t_{n-1})\bar{V} - \tfrac{1}{2}\{\bar{V}^2, \rho_{\text{tot}}(t_{n-1})\}\right)\delta t^2. \end{aligned} \tag{A12}$$

In Eq. (A12) we introduce the notation $\{\bullet, *\} \equiv \bullet * + * \bullet$. By tracing out the nth ancilla, the equation for the reduced dynamics of the giant atoms takes the form

$$\delta\rho_n = -i[H_{\text{eff}} + \langle\bar{V}\rangle, \rho_{n-1}]\delta t + \text{Tr}_n\{(\bar{V}\rho_{n-1}\eta_n\bar{V} - \tfrac{1}{2}\{\bar{V}^2, \rho_{n-1}\eta_n\})\}\delta t^2, \quad \text{(A13)}$$

with $\langle\bar{V}\rangle = \text{Tr}_n\{\bar{V}\eta_n\}$. Using Eq. (A10), the first and second moments for a general white-noise Gaussian state are given by [58]

$$\langle x_n\rangle = \varepsilon_n\sqrt{\delta t}, \quad \langle x_n^\dagger x_{n'}\rangle = N\delta_{n,n'}, \quad \langle x_n x_{n'}\rangle = M\delta_{n,n'}, \quad \text{(A14)}$$

where ε_n is the mean value of $\varepsilon(t)$ on the nth interval, N is the average number of excitations of each ancilla, and M measures its squeezing. For the waveguide driven by a squeezed vacuum field, we have $N = \sinh^2 r$ and $M = e^{-i\phi}\sinh r\cosh r$ with r being the squeezing strength and ϕ the squeezing angle. Based on Eqs. (A14) and considering the continuous-time limit $\gamma\delta t \to 0$, the quantum master equation for the giant atoms is obtained as [24]

$$\begin{aligned}\dot{\rho} = &-i[H_{\text{eff}} + H_d, \rho] \\ &+ \gamma_R\{(N+1)\mathcal{D}_O[\rho] + N\mathcal{D}_{O^\dagger}[\rho]\} \\ &+ \gamma_L\{(N'+1)\mathcal{D}_{O'}[\rho] + N'\mathcal{D}_{O'^\dagger}[\rho]\} \\ &+ \gamma_R\{M(O^\dagger\rho O^\dagger - \tfrac{1}{2}\{O^{\dagger 2}, \rho\}) + \text{H.c.}\} \\ &+ \gamma_L\{M'(O'^\dagger\rho O'^\dagger - \tfrac{1}{2}\{O'^{\dagger 2}, \rho\}) + \text{H.c.}\}, \end{aligned} \quad \text{(A15)}$$

with the coherent driving Hamiltonian

$$H_d = \sqrt{\gamma_R}O^\dagger\varepsilon(t) + \sqrt{\gamma_L}O'^\dagger\varepsilon'(t) + \text{H.c.} \quad \text{(A16)}$$

In this work, we consider that the waveguide is only driven by the squeezed vacuum field and hence $H_d = 0$. Moreover, we assume that $\gamma_R = \gamma_L = \Gamma/2$ (nonchiral case [26]), $N = N'$, and $M = M'$.

For a single giant atom coupled to the waveguide at multiple coupling points, the lowering operators and collective operators of the giant atoms are

$$\begin{aligned} O &= \sigma_-\sum_{n=1}^{\mathcal{P}} e^{-ik_0x_n}, \quad O' = \sigma_-\sum_{n=1}^{\mathcal{P}} e^{ik_0x_n}, \\ O_\alpha &= \sigma_- e^{-ik_0x_\alpha}, \quad O'_\alpha = \sigma_- e^{ik_0x_\alpha}. \end{aligned} \quad \text{(A17)}$$

Substituting Eq. (A17) into Eq. (A15), we obtain the quantum master equation of a single giant atom, as shown in Eq. (3).

For two giant atoms, where each is coupled to the waveguide at two separate points, we have the following operators:

$$\begin{aligned} O &= \sum_{m,n=1,2}\sigma_m^- e^{-ik_0x_{mn}}, \quad O' = \sum_{m,n=1,2}\sigma_m^- e^{ik_0x_{mn}}, \\ O_1 &= \sigma_1^- e^{-ik_0x_{11}}, \quad O'_1 = \sigma_1^- e^{ik_0x_{11}}, \\ O_2 &= \sigma_1^- e^{-ik_0x_{12}}, \quad O'_2 = \sigma_1^- e^{ik_0x_{12}}, \\ O_3 &= \sigma_2^- e^{-ik_0x_{21}}, \quad O'_3 = \sigma_2^- e^{ik_0x_{21}}, \\ O_4 &= \sigma_2^- e^{-ik_0x_{22}}, \quad O'_4 = \sigma_2^- e^{ik_0x_{22}}. \end{aligned} \quad \text{(A18)}$$

Similarly, substituting Eq. (A18) into Eq. (A15) gives the quantum master equation of two giant atoms, as shown in Eq. (7).

APPENDIX B: GENERAL STEADY-STATE SOLUTIONS OF THE QUANTUM MASTER EQUATION

In this Appendix, we present the general steady-state solutions of the quantum master equation (10). Equation (10) shows that both the propagating phase θ_0 and the center-of-mass phase θ_c influence the dynamics of the two giant atoms. In the main text, we have already analyzed the effects of θ_0 (θ_c) on the steady-state population and entanglement by taking typical values of θ_c (θ_0). Since the initial population in the dark state $|+\rangle$ or $|-\rangle$ can modify the steady-state solutions, we exclude such case here. After some lengthy calculations, we obtain

$$\begin{aligned}
\rho_{ee}^\infty &= \frac{N\{h_1(\gamma_c,\Gamma_s)(\gamma_{11}-\gamma_{22})^2 + [4N\delta\omega^2 - h_2(\gamma_c,\Gamma_s)]F(g,\Gamma_s)\}}{(2N+1)^2\{N(N+1)f(\gamma_c,\Gamma_s)(\gamma_{11}-\gamma_{22})^2 + [4\delta\omega^2 - f(\gamma_c,\Gamma_s)]F(g,\Gamma_s)\}}, \\
\rho_{\pm\pm}^\infty &= \frac{N(N+1)\{h_4(\gamma_c,\Gamma_s)(\gamma_{11}-\gamma_{22})^2 + [4\delta\omega^2 - h_3(\gamma_c,\Gamma_s)]F(g,\Gamma_s)\}}{(2N+1)^2\{N(N+1)f(\gamma_c,\Gamma_s)(\gamma_{11}-\gamma_{22})^2 + [4\delta\omega^2 - f(\gamma_c,\Gamma_s)]F(g,\Gamma_s)\}}, \\
\rho_u^\infty &= \frac{2\sqrt{N(N+1)}\Gamma_s\gamma_c[N(N+1)(\gamma_{11}-\gamma_{22})^2 - F(g,\Gamma_s)]}{(2N+1)\{N(N+1)f(\gamma_c,\Gamma_s)(\gamma_{11}-\gamma_{22})^2 + [4\delta\omega^2 - f(\gamma_c,\Gamma_s)]F(g,\Gamma_s)\}}, \\
\rho_v^\infty &= \frac{2i\delta\omega F(g,\Gamma_s)}{(2N+1)\Gamma_s\{N(N+1)(\gamma_{11}-\gamma_{22})^2 - F(g,\Gamma_s)\}}\rho_u, \\
\rho_{+-}^\infty &= \frac{1}{2}\frac{\sqrt{N(N+1)}(\gamma_{11}-\gamma_{22})}{2ig + (2N+1)\Gamma_s}\rho_v, \\
\rho_{-+}^\infty &= \frac{1}{2}\frac{\sqrt{N(N+1)}(\gamma_{11}-\gamma_{22})}{2ig - (2N+1)\Gamma_s}\rho_v.
\end{aligned} \quad \text{(B1)}$$

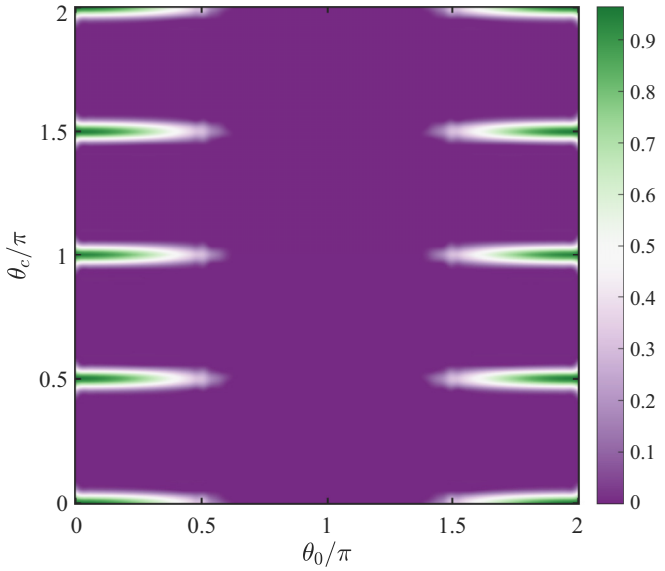

FIG. 8. Steady-state concurrence as a function of θ_0 and θ_c. The other parameter is $r = 1$.

In Eq. (B1), we introduce functions $F(g, \Gamma_s) = (2N + 1)^2\Gamma_s^2 + 4g^2$, $f(\gamma_c, \Gamma_s) = [4N(N + 1)(\gamma_c^2 - \Gamma_s^2) - \Gamma_s^2]$, $h_1(\gamma_c, \Gamma_s) = N(N + 1)(2N + 1)[(N + 1)(2N - 1)\gamma_c^2 - N(2N + 1)\Gamma_s^2]$, $h_2(\gamma_c, \Gamma_s) = (2N + 1)[(N + 1)(2N - 1)\gamma_c^2 - N(2N + 1)\Gamma_s^2]$, $h_3(\gamma_c, \Gamma_s) = (2N + 1)^2(\gamma_c^2 - \Gamma_s^2)$, and $h_4(\gamma_c, \Gamma_s) = N(N + 1)h_3(\gamma_c, \Gamma_s)$. From these expressions, it can be found that the steady-state populations in the states $|\pm\rangle$ are identical. Different from Eqs. (11) and (12), the steady-state solutions in Eq. (B1) are influenced by the individual decay, individual squeezing, collective squeezing, and the dipole-dipole interaction. Figure 8 shows the steady-state concurrence as a function of θ_0 and θ_c at fixed $r = 1$. We see that C_∞ exhibits a periodic dependence on both θ_0 and θ_c, with higher concurrence values appearing narrow regions of the parameter space. Most of the parameter space corresponds to lower concurrence. This indicates that achieving larger entanglement of the two giant atoms requires careful tuning of the values of these two phases.

[1] A. F. Kockum, Quantum optics with giant atoms—The first five years, in *International Symposium on Mathematics, Quantum Theory, and Cryptography*, edited by T. Takagi, M. Wakayama, K. Tanaka, N. Kunihiro, K. Kimoto, and Y. Ikematsu (Springer Singapore, Singapore, 2021), pp. 125–146.

[2] B. Kannan, M. Ruckriegel, D. Campbell, A. F. Kockum, J. Braumüller, D. Kim, M. Kjaergaard, P. Krantz, A. Melville, B. M. Niedzielski, A. Vepsäläinen, R. Winik, J. Yoder, F. Nori, T. P. Orlando, S. Gustavsson, and W. D. Oliver, Waveguide quantum electrodynamics with superconducting artificial giant atoms, Nature (London) **583**, 775 (2020).

[3] C. Joshi, F. Yang, and M. Mirhosseini, Resonance fluorescence of a chiral artificial atom, Phys. Rev. X **13**, 021039 (2023).

[4] J.-J Hu, D.-F. Li, Y.-F. Qie, Z.-L. Yin, A. F. Kockum, F. Nori, and S.-M. An, Engineering the environment of a superconducting qubit with an artificial giant atom, arXiv:2410.15377.

[5] M. V. Gustafsson, T. Aref, A. F. Kockum, M. K. Ekstrm, G. Johansson, and P. Delsing, Propagating phonons coupled to an artificial atom, Science **346**, 207 (2014).

[6] R. Manenti, A. F. Kockum, A. Patterson, T. Behrle, J. Rahamim, G. Tancredi, F. Nori, and P. J. Leek, Circuit quantum acoustodynamics with surface acoustic waves, Nat. Commun. **8**, 975 (2017).

[7] G. Andersson, B. Suri, L. Guo, T. Aref, and P. Delsing, Nonexponential decay of a giant artificial atom, Nat. Phys. **15**, 1123 (2019).

[8] Z. Liao, X. Zeng, H. Nha, and M. S. Zubairy, Photon transport in a one-dimensional nanophotonic waveguide QED system, Phys. Scr. **91**, 063004 (2016).

[9] D. Roy, C. M. Wilson, and O. Firstenberg, *Colloquium*: Strongly interacting photons in one-dimensional continuum, Rev. Mod. Phys. **89**, 021001 (2017).

[10] X. Gu, A. F. Kockum, A. Miranowicz, Y.-x. Liu, and F. Nori, Microwave photonics with superconducting quantum circuits, Phys. Rep. **718**, 1 (2017).

[11] A. S. Sheremet, M. I. Petrov, I. V. Iorsh, A. V. Poshakinskiy, and A. N. Poddubny, Waveguide quantum electrodynamics: Collective radiance and photon-photon correlations, Rev. Mod. Phys. **95**, 015002 (2023).

[12] A. F. Kockum, P. Delsing, and G. Johansson, Designing frequency-dependent relaxation rates and Lamb shifts for a giant artificial atom, Phys. Rev. A **90**, 013837 (2014).

[13] A. M. Vadiraj, A. Ask, T. G. McConkey, I. Nsanzineza, C. W. S. Chang, A. F. Kockum, and C. M. Wilson, Engineering the level structure of a giant artificial atom in waveguide quantum electrodynamics, Phys. Rev. A **103**, 023710 (2021).

[14] L. Guo, A. Grimsmo, A. F. Kockum, M. Pletyukhov, and G. Johansson, Giant acoustic atom: A single quantum system with a deterministic time delay, Phys. Rev. A **95**, 053821 (2017).

[15] S. Longhi, Photonic simulation of giant atom decay, Opt. Lett. **45**, 3017 (2020).

[16] L. Du, M.-R. Cai, J.-H. Wu, Z. Wang, and Y. Li, Single-photon nonreciprocal excitation transfer with non-Markovian retarded effects, Phys. Rev. A **103**, 053701 (2021).

[17] L. Du, Y.-T. Chen, Y. Zhang, and Y. Li, Giant atoms with time-dependent couplings, Phys. Rev. Res. **4**, 023198 (2022).

[18] X.-L. Yin, W.-B. Luo, and J.-Q. Liao, Non-Markovian disentanglement dynamics in double-giant-atom waveguide-QED systems, Phys. Rev. A **106**, 063703 (2022).

[19] Q.-Y. Qiu, Y. Wu, and X.-Y. Lü, Collective radiance of giant atoms in non-Markovian regime, Sci. Chin. Phys. Mech. Astron. **66**, 224212 (2023).

[20] L. Xu and L. Guo, Catch and release of propagating bosonic field with non-Markovian giant atom, New J. Phys. **26**, 013025 (2024).

[21] F. Roccati and D. Cilluffo, Controlling Markovianity with chiral giant atoms, Phys. Rev. Lett. **133**, 063603 (2024).

[22] Q.-Y. Qiu and X.-Y. Lü, Non-Markovian collective emission of giant emitters in the Zeno regime, Phys. Rev. Res. **6**, 033243 (2024).

[23] A. F. Kockum, G. Johansson, and F. Nori, Decoherence-free interaction between giant atoms in waveguide quantum electrodynamics, Phys. Rev. Lett. **120**, 140404 (2018).

[24] D. Cilluffo, A. Carollo, S. Lorenzo, J. A. Gross, G. M. Palma, and F. Ciccarello, Collisional picture of quantum optics with giant emitters, Phys. Rev. Res. **2**, 043070 (2020).

[25] A. Carollo, D. Cilluffo, and F. Ciccarello, Mechanism of decoherence-free coupling between giant atoms, Phys. Rev. Res. **2**, 043184 (2020).

[26] A. Soro and A. F. Kockum, Chiral quantum optics with giant atoms, Phys. Rev. A **105**, 023712 (2022).

[27] L. Du, L. Z. Guo, and Y. Li, Complex decoherence-free interactions between giant atoms, Phys. Rev. A **107**, 023705 (2023).

[28] L. Guo, A. F. Kockum, F. Marquardt, and G. Johansson, Oscillating bound states for a giant atom, Phys. Rev. Res. **2**, 043014 (2020).

[29] X. Wang, T. Liu, A. F. Kockum, H.-R. Li, and F. Nori, Tunable chiral bound states with giant atoms, Phys. Rev. Lett. **126**, 043602 (2021).

[30] C. Vega, M. Bello, D. Porras, and A. González-Tudela, Qubit-photon bound states in topological waveguides with long-range hoppings, Phys. Rev. A **104**, 053522 (2021).

[31] W. Cheng, Z. Wang, and Y.-X. Liu, Topology and retardation effect of a giant atom in a topological waveguide, Phys. Rev. A **106**, 033522 (2022).

[32] H. Xiao, L. Wang, Z.-H. Li, X. Chen, and L. Yuan, Bound state in a giant atom-modulated resonators system, npj Quantum Inf. **8**, 80 (2022).

[33] K. H. Lim, W. K. Mok, and L. C. Kwek, Oscillating bound states in non-Markovian photonic lattices, Phys. Rev. A **107**, 023716 (2023).

[34] X. Wang, H.-B. Zhu, T. Liu, and F. Nori, Realizing quantum optics in structured environments with giant atoms, Phys. Rev. Res. **6**, 013279 (2024).

[35] W. Zhao and Z. Wang, Single-photon scattering and bound states in an atom-waveguide system with two or multiple coupling points, Phys. Rev. A **101**, 053855 (2020).

[36] L. Du and Y. Li, Single-photon frequency conversion via a giant Λ-type atom, Phys. Rev. A **104**, 023712 (2021).

[37] Q. Y. Cai and W. Z. Jia, Coherent single-photon scattering spectra for a giant-atom waveguide-QED system beyond the dipole approximation, Phys. Rev. A **104**, 033710 (2021).

[38] S. L. Feng and W. Z. Jia, Manipulating single-photon transport in a waveguide-QED structure containing two giant atoms, Phys. Rev. A **104**, 063712 (2021).

[39] J.-P. Zou, R.-Y. Gong, and Z.-L. Xiang, Tunable single-photon scattering of a giant Λ-type atom in a SQUID-chain waveguide, Font. Phys. **10**, 896827 (2022).

[40] X.-L. Yin, Y.-H. Liu, J.-F. Huang, and J.-Q. Liao, Single-photon scattering in a giant-molecule waveguide-QED system, Phys. Rev. A **106**, 013715 (2022).

[41] W. Gu, H. Huang, Z. Yi, L. Chen, L. Sun, and H. Tan, Correlated two-photon scattering in a one-dimensional waveguide coupled to two- or three-level giant atoms, Phys. Rev. A **108**, 053718 (2023).

[42] W. Gu, L. Chen, Z. Yi, S. Liu, and G.-X. Li, Tunable photonphoton correlations in waveguide QED systems with giant atoms, Phys. Rev. A **109**, 023720 (2024).

[43] A. C. Santos and R. Bachelard, Generation of maximally entangled long-lived states with giant atoms in a waveguide, Phys. Rev. Lett. **130**, 053601 (2023).

[44] X.-L. Yin and J.-Q. Liao, Generation of two-giant-atom entanglement in waveguide-QED systems, Phys. Rev. A **108**, 023728 (2023).

[45] Y.-T. Chen, L. Du, Y. Zhang, L. Guo, J.-H. Wu, M. Artoni, and G. C. La Rocca, Giant-atom effects on population and entanglement dynamics of Rydberg atoms in the optical regime, Phys. Rev. Res. **5**, 043135 (2023).

[46] M. Weng, X. Wang, and Z. Wang, Interaction and entanglement engineering in a driven-giant-atom setup with a coupled resonator waveguide, Phys. Rev. A **110**, 023721 (2024).

[47] J. B. You, J. F. Kong, D. Aghamalyan, W. K. Mok, K. H. Lim, J. Ye, C. E. Png, and F. J. Garcia-Vidal, Generation and optimization of entanglement between giant atoms chirally coupled to spin cavities, arXiv:2403.00264.

[48] W.-B. Luo, X.-L. Yin, and J.-Q. Liao, Entangling two giant atoms via a topological waveguide, Adv. Quantum Technol. **7**, 2400030 (2024).

[49] C. W. Gardiner, Inhibition of atomic phase decays by squeezed light: A direct effect of squeezing, Phys. Rev. Lett. **56**, 1917 (1986).

[50] H. J. Carmichael, A. S. Lane, and D. F. Walls, Resonance fluorescence from an atom in a squeezed vacuum, Phys. Rev. Lett. **58**, 2539 (1987).

[51] D. M. Toyli, A. W. Eddins, S. Boutin, S. Puri, D. Hover, V. Bolkhovsky, W. D. Oliver, A. Blais, and I. Siddiqi, Resonance fluorescence from an artificial atom in squeezed vacuum, Phys. Rev. X **6**, 031004 (2016).

[52] Z. Ficek, Spontaneous emission from two atoms interacting with a broadband squeezed vacuum, Phys. Rev. A **42**, 611 (1990).

[53] E. V. Goldstein and P. Meystre, Dipole-dipole interaction in squeezed vacua, Phys. Rev. A **53**, 3573 (1996).

[54] J. You, Z. Liao, S.-W. Li, and M. S. Zubairy, Waveguide quantum electrodynamics in squeezed vacuum, Phys. Rev. A **97**, 023810 (2018).

[55] J. You, Z. Liao, and M. S. Zubairy, Steady-state population inversion of multiple Θ-type emitters by the squeezed vacuum in a waveguide, Phys. Rev. A **100**, 013843 (2019).

[56] S.-Y. Bai and J.-H. An, Generating stable spin squeezing by squeezed-reservoir engineering, Phys. Rev. Lett. **127**, 083602 (2021).

[57] R. Gutiérrez-Jáuregui, A. Asenjo-Garcia, and G. S. Agarwal, Dissipative stabilization of dark quantum dimers via squeezed vacuum, Phys. Rev. Res. **5**, 013127 (2023).

[58] F. Ciccarello, S. Lorenzo, V. Giovannetti, and G. M. Palma, Quantum collision models: Open system dynamics from repeated interactions, Phys. Rep. **954**, 1 (2022).

[59] H.-P. Breuer and F. Petruccione, *The Theory of Open Quantum Systems* (Oxford University Press, Oxford, 2002).

[60] J. Gough and M. R. James, Quantum feedback networks: Hamiltonian formulation, Commun. Math. Phys. **287**, 1109 (2009).

[61] J. Gough and M. R. James, The series product and its application to quantum feedforward and feedback networks, IEEE Trans. Autom. Control **54**, 2530 (2009).
[62] G. Zhang and M. R. James, Quantum feedback networks and control: A brief survey, Chin. Sci. Bull. **57**, 2200 (2012).
[63] M. O. Scully and M. S. Zubairy, *Quantum Optics* (Cambridge University Press, Cambridge, 1997).
[64] G. Lindblad, On the generators of quantum dynamical semigroups, Commun. Math. Phys. **48**, 119 (1976).
[65] S. Das, G. S. Agarwal, and M. O. Scully, Quantum interferences in cooperative Dicke emission from spatial variation of the laser phase, Phys. Rev. Lett. **101**, 153601 (2008).
[66] C. W. Gardiner and P. Zoller, *Quantum Noise: A Handbook of Markovian and Non-Markovian Quantum Stochastic Methods with Applications to Quantum Optics* (Springer, Berlin, 2004).
[67] E. Schrödinger, The current situation in quantum mechanics, Naturwissenschaften **23**, 807 (1935).
[68] A. Einstein, B. Podolsky, and N. Rosen, Can quantum-mechanical description of physical reality be considered complete? Phys. Rev. **47**, 777 (1935).
[69] R. Horodecki, P. Horodecki, M. Horodecki, and K. Horodecki, Quantum entanglement, Rev. Mod. Phys. **81**, 865 (2009).
[70] A. González-Tudela, D. Martin-Cano, E. Moreno, L. Martin-Moreno, C. Tejedor, and F. J. Garcia-Vidal, Entanglement of two qubits mediated by one-dimensional plasmonic waveguides, Phys. Rev. Lett. **106**, 020501 (2011).
[71] H. Zheng and H. U. Baranger, Persistent quantum beats and long-distance entanglement from waveguide-mediated interactions, Phys. Rev. Lett. **110**, 113601 (2013).
[72] A. González-Tudela and D. Porras, Mesoscopic entanglement induced by spontaneous emission in solid-state quantum optics, Phys. Rev. Lett. **110**, 080502 (2013).
[73] C. Gonzalez-Ballestero, E. Moreno, and F. J. G. Vidal, Generation, manipulation, and detection of two-qubit entanglement in waveguide QED, Phys. Rev. A **89**, 042328 (2014).
[74] P. Facchi, M. S. Kim, S. Pascazio, F. V. Pepe, D. Pomarico, and T. Tufarelli, Bound states and entanglement generation in waveguide quantum electrodynamics, Phys. Rev. A **94**, 043839 (2016).
[75] T. Ramos, H. Pichler, A. J. Daley, and P. Zoller, Quantum spin dimers from chiral dissipation in cold-atom chains, Phys. Rev. Lett. **113**, 237203 (2014).
[76] C. Gonzalez-Ballestero, A. Gonzalez-Tudela, F. J. Garcia-Vidal, and E. Moreno, Chiral route to spontaneous entanglement generation, Phys. Rev. B **92**, 155304 (2015).
[77] I. M. Mirza and J. C. Schotland, Multiqubit entanglement in bidirectional-chiral-waveguide QED, Phys. Rev. A **94**, 012302 (2016).
[78] W. K. Mok, J. B. You, L. C. Kwek, and D. Aghamalyan, Microresonators enhancing long-distance dynamical entanglement generation in chiral quantum networks, Phys. Rev. A **101**, 053861 (2020).
[79] P. S. Shah, F. Yang, C. Joshi, and M. Mirhosseini, Stabilizing remote entanglement via waveguide dissipation, PRX Quantum **5**, 030346 (2024).
[80] W. K. Wootters, Entanglement of formation of an arbitrary state of two qubits, Phys. Rev. Lett. **80**, 2245 (1998).
[81] X. Ge, L. Liu, Y. Wang, Y. Xiang, G. Zhang, L. Li, and S. Cheng, Faithful geometric measures for genuine tripartite entanglement, Phys. Rev. A **110**, L010402 (2024).
[82] L. Mazzola, S. Maniscalco, J. Piilo, K.-A. Suominen, and B. M. Garraway, Sudden death and sudden birth of entanglement in common structured reservoirs, Phys. Rev. A **79**, 042302 (2009).
[83] J. León and C. Sabín, Photon exchange and correlation transfer in atom-atom entanglement dynamics, Phys. Rev. A **79**, 012301 (2009).
[84] Z. Q. Wang, Y. P. Wang, J. Yao, R. C. Shen, W. J. Wu, J. Qian, J. Li, S. Y. Zhu, and J. Q. You, Giant spin ensembles in waveguide magnonics, Nat. Commun. **13**, 7580 (2022).
[85] L. Du, Y. Zhang, J. H. Wu, A. F. Kockum, and Y. Li, Giant atoms in a synthetic frequency dimension, Phys. Rev. Lett. **128**, 223602 (2022).
[86] A. González-Tudela, C. S. Muñoz, and J. I. Cirac, Engineering and harnessing giant atoms in high-dimensional baths: A proposal for implementation with cold atoms, Phys. Rev. Lett. **122**, 203603 (2019).
[87] M. A. Castellanos-Beltran, K. D. Irwin, G. C. Hilton, L. R. Vale, and K. W. Lehnert, Amplification and squeezing of quantum noise with a tunable Josephson metamaterial, Nat. Phys. **4**, 929 (2008).
[88] J. Bourassa, F. Beaudoin, J. M. Gambetta, and A. Blais, Josephson-junction-embedded transmission-line resonators: From Kerr medium to in-line transmon, Phys. Rev. A **86**, 013814 (2012).
[89] H. Vahlbruch, M. Mehmet, K. Danzmann, and R. Schnabel, Detection of 15 dB squeezed states of light and their application for the absolute calibration of photoelectric quantum efficiency, Phys. Rev. Lett. **117**, 110801 (2016).
[90] T. Serikawa, J.-I. Yoshikawa, K. Makino, and A. Frusawa, Creation and measurement of broadband squeezed vacuum from a ring optical parametric oscillator, Opt. Express **24**, 28383 (2016).
[91] J.-T. Shen and S. Fan, Coherent single photon transport in a one-dimensional waveguide coupled with superconducting quantum bits, Phys. Rev. Lett. **95**, 213001 (2005).
[92] J.-T. Shen and S. Fan, Theory of single-photon transport in a single-mode waveguide. I. Coupling to a cavity containing a two-level atom, Phys. Rev. A **79**, 023837 (2009).
[93] C. W. Gardiner and M. J. Collett, Input and output in damped quantum systems: Quantum stochastic differential equations and the master equation, Phys. Rev. A **31**, 3761 (1985).